ELSEVIER

Coordination Chemistry Reviews
209 (2000) 161–196

COORDINATION CHEMISTRY REVIEWS

www.elsevier.com/locate/ccr

Ligating ability of 1,1′-bis(diphenylphosphino)ferrocene: a structural survey (1994–1998)

Giuliano Bandoli *, Alessandro Dolmella

Università di Padova, Dipartimento di Scienze Farmaceutiche, Via F. Marzolo 5, I-35131 Padua, Italy

Received 9 August 1999; received in revised form 8 November 1999; accepted 14 December 1999

Contents

Abbreviations: Arylamine, *p*-$MeOC_6H_3CH{=}N\text{-}CH_2\text{-}\overline{CHCH_2CH_2CHC(Me_2)}CHCH_2$; bipy, 2,2′-bipyridine; bph, biphenyl (2−); clan, 9-(10-chloroanthracenide) (1−); cod, 1,5-cyclooctadiene; Cp, η^5-cyclopentadienyl; Cp*, η^5-pentamethylcyclopentadienide (1−); dbsq, 3,6-di-tert-butyl-*o*-benzosemiquinone (1−); dppf, 1,1′-bis(diphenylphosphino)ferrocene; Et, ethyl; Et_2O, diethyl ether; $H_2norpcS_2$, (norphtalocyanine)-2,3-dithiolate (2−); Me, methyl; Me_2CO, acetone; Me_2pz, 3,5-dimethylpyrazolate (1−); OTf, triflate (1−); pa, pyridine-2-carbaldehyde azine; pdt, 1,3-propanedithiolate (2−); Ph, phenyl; phen, 1,10-phenanthroline; pms, *p*-methoxystyrenyl; pz, pyrazolate (1−); Spy, 2-pyridinethiolate (1−); THF, tetrahydrofuran; thiaz, 2,3-dimethylthiazolium (1+); Tos, tosyl.

* Corresponding author. Tel.: +39-49-827-5344; fax: +39-49-827-5345 (5366).
E-mail address: bandoli@dsfarm.unipd.it (G. Bandoli)

0010-8545/00/$ - see front matter
PII: S0010-8545(00)00229-0

Abstract

This paper outlines the ligating ability of 1,1′-bis(diphenylphosphino) ferrocene. The focus is on the extensive coordination chemistry exhibited by this ligand to transition metals. The structural parameters of mono-, bi- and polynuclear species are reviewed and simple relationships between some of these parameters are reported and discussed. The review mainly covers the X-ray structure determinations published over the 1994–98 period.

Keywords: 1,1′-Bis(diphenylphosphino)ferrocene (dppf); Mononuclear complexes; Polynuclear complexes; X-ray structure

1. Introduction

The first structure determination of a dppf (Fig. 1) complex was reported in 1984 ([Pd(dppf)Cl_2] [1]); the first example of a dppf-containing cluster was described in 1989 ([Co_3(μ-dppf)(μ_3-CCH_3)$(CO)_7$] [2]).

Overall, 56 X-ray structure determinations of complexes and clusters containing the dppf ligand appeared in the literature between 1984 and 1993. These and other data are shown in the fundamental and excellent book 'Ferrocenes' [3]. In the following 5 years (1994–1998) 97 more structures of dppf-containing compounds were reported; 74 were monomeric complexes and compounds without metal–metal bonds, and 23 were clusters. The figures clearly indicate the ever-increasing appeal

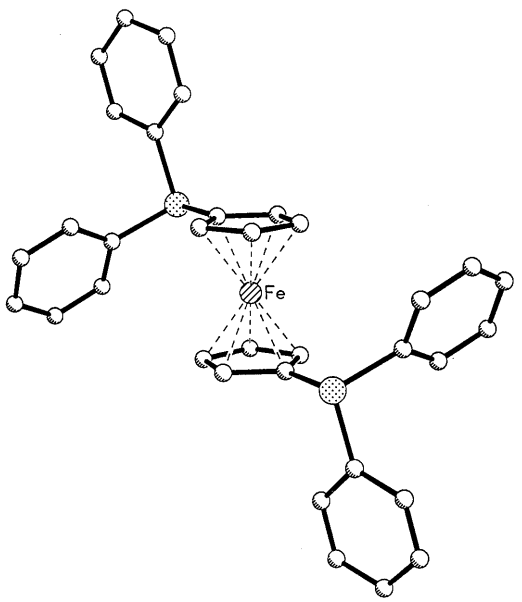

Fig. 1. The dppf ligand.

of this peculiar domain of coordination and organometallic chemistry. The present work deals with solid-state structure determinations of dppf complexes with transition metal elements and those comprising the zinc–triad that appeared between 1994 and 1998. However, this paper does not examine clusters, which have already been largely discussed (up to 1997) in the brilliant and recent review presented by Fong and Hor [4]. Some aspects of the rich scientific documentation produced in the 1994–98 period are highlighted in Fig. 2. Fig. 2a shows how many structures have been published each year and Fig. 2b indicates the Group of the Periodic Table to which the dppf-coordinated atom/atoms belongs/belong. This review also deals with six structure determinations published before 1994 but not included in [3], as well as with ten more structures that appeared in early 1999.

In this work complexes have been classified according to their nuclearity, and arranged in order of (i) increasing number of the Periodic Table Group of metal center/s and (ii) complexity of the coordination sphere. The raw data on which the review is based have been recovered from Chemical Abstracts, but all major pertinent chemistry journals have been independently investigated as well. In the first step, the Cambridge Crystallographic Data Base (version 5.17 of April 1999) has been extensively searched [5]. The considerable research attention granted in recent years to ferrocenyl diphosphine ligands, especially dppf, is due to (i) the various coordination modes towards metal atoms [3,6], (ii) the possible catalytic activity of many of their complexes [3,7], (iii) the redox chemistry of their complexes [8,9] and also (iv) the chemotherapeutic potential for cancer treatment [10]. With respect to the mode of numbering for the complexes, in this work they are numbered according to their reference. If more than one structure is reported in the same paper, as in [46], where three complexes are described, they are labeled as [46a–c].

2. Coordinating modes of dppf

The coordination versatility of the metalloligand 1,1′-bis(diphenylphosphino)ferrocene is highly remarkable. Actually, the various coordinating modes of dppf just reflect its ability to change conformation in order to match the steric demands of the surrounding molecular environment. Nevertheless, dppf acts mainly as a η^2-mode diphosphine ligand. Excluding clusters, in fact, 59 of the 90 structures discussed in this review (65.5%) are mononuclear complexes containing one (53) or two (6) η^2-chelating dppf ligand(s) (Tables 1 and 2), but the same binding mode is also found in many polynuclear complexes. With a single exception (see Section 6), the unidentate η^1-mode has not been structurally characterized in the last 5 years, despite its previous occurrence in compounds such as Fe(η^1-dppf)$(CO)_4$ [11] and the series M(η^1-dppf)$(CO)_5$ (M = Cr, Mo, W) [12,13]; likewise, there are no examples of dppf acting as a tridentate ligand. Usually, no formal ferrocenyl–metal interaction occurs, a direct interaction between the ferrocenyl iron and the phosphine-bound metal center was first reported in the mononuclear complex $[Pd(dppf)(PPh_3)][BF_4]_2$ [14] and later confirmed by an electronic spectrum [15]. Another occurrence of

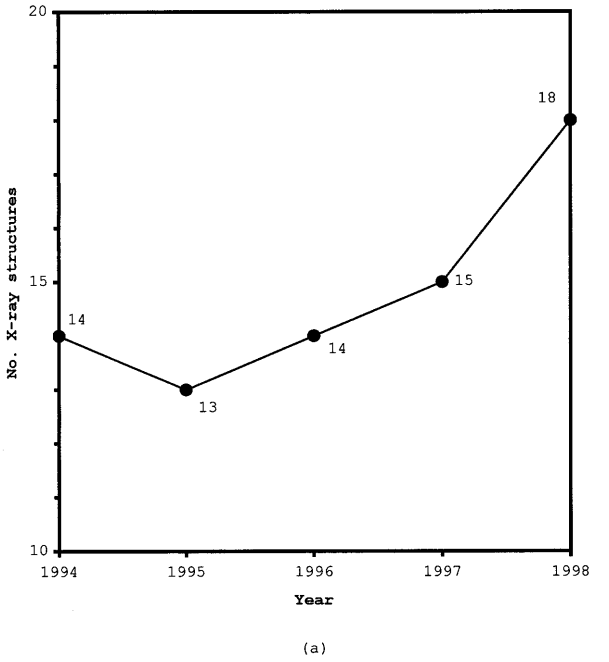

(a)

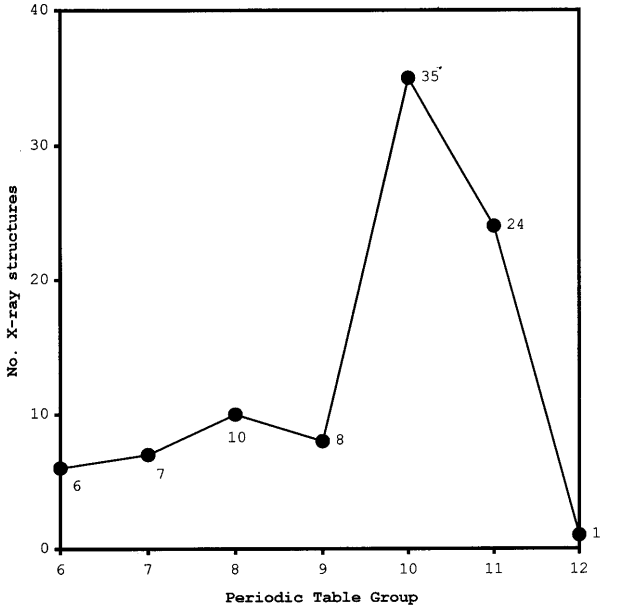

(b)

Fig. 2. (a) Number of X-ray structures per year; (b) distribution of X-ray structures across the Periodic Table.

Table 1
Relevant structural parameters for mononuclear complexes containing a η^2-chelating dppf ligand

Complex	τ (°)	Θ (°)	$X_A \cdots Fe \cdots X_B$ (°)	P···Fe···P (°)	P···P (Å)	M–P (Å)	P–M–P (°)	Fe···M (Å)	Ref.
Group 6									
$[Mo(dppf)(CO)_4]$[a]	52.9	2.7	179.2	70.8	3.88	2.561(3), 2.594(3)	97.7(1)	4.43	[19]
	37.5	2.4	178.3	66.4	3.76	2.572(3), 2.537(3)	94.9(1)	4.55	
$[W(dppf)(CO)_3(NCMe)]$	50.1	2.5	179.7	68.7	3.82	2.539(2), 2.539(2)	97.4(1)	4.46	[20]
$[W(dppf)(CO)_2Cl(CPh)]$	44.6	1.9	178.2	69.5	3.90	2.583(2), 2.585(2)	97.8(1)	4.50	[21]
Group 7									
$[Mn(dppf)(CO)_3H]$	26.8	5.2	177.2	60.1	3.43	2.313(1), 2.304(1)	95.9(1)	4.36	[22a]
$[Mn(dppf)(CO)_3Cl]$	13.6	0.8	178.0	61.3	3.53	2.387(1), 2.405(2)	95.0(1)	4.44	[22b]
$[Mn(dppf)(CO)(\eta^5\text{-}MeC_5H_4)]\cdot CH_2Cl_2$, isomer i	0.0	4.6	176.7	58.1	3.38	2.233(2), 2.196(2)	99.4(1)	4.27	[23a]
$[Mn(dppf)(CO)(\eta^5\text{-}MeC_5H_4)]\cdot CH_2Cl_2$, isomer ii	5.6	2.6	178.0	57.9	3.36	2.227(2), 2.210(2)	98.7(1)	4.30	[23b]
Group 8									
$[Fe(dppf)(NO)_2]$	37.6	3.0	178.3	62.4	3.50	2.264(2), 2.256(2)	101.7(1)	4.20	[24a]
[Ru(dppf)H(Cp*)]	40.5	7.2	176.0	60.2	3.42	2.272(1), 2.259(1)	97.9(1)	4.38	[25]
$[Ru(dppf)(\eta^6\text{-}Me_6C_6)Cl][PF_6]$	3.9	3.7	178.1	58.4	3.41	2.361(3), 2.376(3)	92.0(1)	4.49	[26a]
$[Ru(dppf)(\eta^6\text{-}p\text{-cymene})Cl][PF_6]$	1.3	1.8	179.1	59.5	3.46	2.383(3), 2.352(3)	93.7(1)	4.47	[27]
$[Ru(dppf)(\eta^2\text{-}O_2)(Cp^*)][BF_4]$	10.9	5.2	175.8	59.4	3.44	2.407(3), 2.390(3)	91.6(1)	4.40	[28]
$[Ru(dppf)(bipy)_2][PF_6]_2$[b]	24.1	1.6	178.3	63.4	3.67	2.393(2)	100.3(1)	4.51	[29]
$[Ru(dppf)(CO)(PPh_3)ClH]$	50.2	3.0	178.9	69.3	3.82	2.518(4), 2.392(4)	102.2(1)	4.30	[30]
$[Ru(dppf)(CO)(NCMe)(PPh_3)H][BF_4]\cdot EtOH$	51.4	4.8	176.8	68.1	3.79	2.508(3), 2.367(3)	102.1(1)	4.33	[31]
Group 9									
$[Co(dppf)(NO)_2][SbF_6]$	28.7	0.6	177.6	64.5	3.66	2.276(4), 2.300(4)	106.2(1)	4.26	[32]
$[Ir(dppf)(\eta^4\text{-cod})][PF_6]$	41.4	3.2	179.0	64.9	3.58	2.345(3), 2.359(3)	99.2(1)	4.34	[33]

Table 1 (*Continued*)

Complex	τ (°)	Θ (°)	$X_A\cdots Fe\cdots X_B$ (°)	P···Fe···P (°)	P···P (Å)	M–P (Å)	P–M–P (°)	Fe···M (Å)	Ref.
Group 10									
$[Pd(dppf)Cl_2]\cdot CH_2Cl_2$	34.1	6.7	176.6	61.5	3.43	2.291(8), 2.262(4)	97.8(2)	4.23	[34a]
$[Pd(dppf)(H_2norpcS_2)]$	34.6	4.1	178.8	61.8	3.49	2.322(4), 2.309(4)	97.9(5)	4.27	[36]
[Pd(dppf)Br(clan)]	37.2	1.5	179.4	63.7	3.58	2.401(2), 2.272(2)	99.8(1)	4.27	[37]
$[Pd(dppf)Br(\eta^1\text{-}C_5H_4NH\text{–}C^2)]Br\cdot 1/2$ MeOH	45.3	3.3	179.1	65.7	3.63	2.386(1), 2.283(1)	102.1(1)	4.25	[38]
$[Pd(dppf)I(o\text{-}C_6H_4\text{–}CH_2\text{–}O\text{–}CH{=}CH_2]\cdot$ $1/4\ Et_2O\cdot 1/4$ THF	32.1	2.6	179.2	63.5	3.60	2.384(2), 2.287(2)	100.7(1)	4.33	[39]
$[Pd(dppf)(p\text{-}N(CH_3)_2C_6H_4)$ $(N(p\text{-}CH_3C_6H_4)_2]\cdot 3/4\ Me_2CO$	39.4	2.7	179.5	64.3	3.60	2.392(2), 2.283(2)	100.5(1)	4.32	[40]
$[Pd(dppf)(C_{18}H_{24}O_8)]\cdot Me_2CO$, one enantiomer[b]	41.8	4.0	178.6	64.3	3.60	2.386(2)	98.0(1)	4.43	[41a]
$[Pd(dppf)(C_{18}H_{24}O_8)]$, racemate	41.6	3.8	179.3	64.7	3.63	2.390(2), 2.381(2)	98.9(1)	4.41	[41b]
$[Pd(dppf)(o\text{-}MeC_6H_4)(NH\text{–}N{=}CPh_2)]$	29.9	2.9	179.5	62.4	3.57	2.393(3), 2.374(4)	99.8(1)	4.35	[42]
$[Pt(dppf)Cl_2]$	32.0	5.0	176.5	61.1	3.44	2.254(5), 2.266(5)	99.0(2)	4.27	[34b]
$[Pt(dppf)I_2]\cdot 1/3\ CH_2Cl_2$	39.0	6.7	176.9	62.6	3.51	2.282(4), 2.284(4)	100.6(1)	4.27	[43a]
[Pt(dppf)(*trans*-stilbene)]·THF	44.5	3.0	178.2	65.1	3.61	2.264(3), 2.262(3)	105.9(1)	4.19	[44]
[Pt(dppf)(bph)][a]	42.9	4.9	177.1	62.9	3.54	2.340(7), 2.337(5)	98.3(2)	4.38	[45a]
	46.3	5.1	177.6	64.0	3.56	2.334(5), 2.340(5)	99.0(2)	4.34	
$[Pt(dppf)(bph)]\cdot 2\ CH_2Cl_2$	42.8	6.3	177.1	62.8	3.52	2.316(2), 2.320(2)	98.6(1)	4.38	[45b]
$[Pt(dppf)(Ph)_2]\cdot CH_2Cl_2$	37.0	2.9	179.4	63.5	3.58	2.316(1), 2.310(1)	101.2(1)	4.35	[43b]
$[Pt(dppf)(pz)_2]$[a]	39.6	5.5	178.1	61.9	3.45	2.283(3), 2.273(2)	98.3(1)	4.19	[46a]
	38.1	6.1	177.9	61.2	3.42	2.276(3), 2.283(3)	97.1(1)	4.22	
$[Pt(dppf)(Me_2pz)_2]$[a]	41.9	7.2	178.9	63.0	3.52	2.273(8), 2.269(9)	101.5(3)	4.31	[46b]
	38.8	5.5	177.9	61.0	3.43	2.267(9), 2.292(9)	97.6(3)	4.17	
$[Pt(dppf)(OH_2)_2][OTf]_2$	30.5	5.2	177.9	60.2	3.37	2.243(2), 2.246(2)	97.4(1)	4.16	[47]
$[Pt(dppf)(C(O)OMe)_2)]\cdot MeOH$	36.0	3.2	179.1	62.0	3.49	2.311(5), 2.331(5)	97.3(2)	4.22	[48]
$[Pt(dppf)(O_2CMe)_2]\cdot H_2O$	34.6	5.6	177.3	60.6	3.40	2.242(1), 2.260(1)	97.9(1)	4.21	[49a]
$[Pt(dppf)(O_2CPh)_2]\cdot CH_2Cl_2$	34.3	1.9	179.1	60.6	3.38	2.219(3), 2.262(3)	98.1(1)	4.16	[49b]

Table 1 (*Continued*)

Complex	τ (°)	Θ (°)	$X_A \cdots Fe \cdots X_B$ (°)	P···Fe···P (°)	P···P (Å)	M–P (Å)	P–M–P (°)	Fe···M (Å)	Ref.
$[Pt(dppf)(thiaz)][BF_4]$	31.2	3.0	177.7	61.9	3.48	2.293(2), 2.354(1)	96.8(1)	4.17	[50a]
$[Pt(dppf)Cl\{\sigma\text{-}C(CH_2)C(Et)=CH_2\}]$	30.1	3.5	178.5	61.6	3.49	2.327(5), 2.224(5)	100.3(2)	4.30	[51]
$[Pt(dppf)Cl(NOsO_3)]$[a]	32.5	3.1	179.3	61.8	3.46	2.270(4), 2.265(5)	99.6(2)	4.22	[52]
	31.6	6.1	176.5	61.1	3.42	2.250(5), 2.288(5)	97.7(2)	4.24	
$[Pt(dppf)(\mu\text{-}pz)_2CdI_2]\cdot 9/20\ CH_2Cl_2$	35.2	5.1	178.1	61.8	3.46	2.282(3), 2.278(3)	98.8(1)	4.26	[46c]
Group 11									
$[Cu(dppf)(dbsq)]\cdot 1/2$ *n*-hexane	45.5	1.0	179.5	66.5	3.71	2.218(1), 2.237(1)	112.9(1)	4.05	[53]
$[Cu(dppf)(\eta^2\text{-}H_2)BH_2]\cdot 2\ C_6H_6$	41.2	3.1	177.2	66.7	3.74	2.249(2), 2.246(2)	112.7(1)	4.09	[54]
$[Ag(dppf)(PPh_3)][ClO_4]\cdot 2\ CH_2Cl_2$	56.0	0.2	178.3	73.2	4.02	2.432(1), 2.480(1)	109.6(1)	4.10	[55a]
$[Ag(dppf)(phen)][ClO_4]$	57.0	1.8	178.5	73.5	4.04	2.411(1), 2.508(1)	110.6(1)	4.09	[55b]
$[Au(dppf)(PPh_3)][ClO_4]\cdot CHCl_3$	54.8	1.3	178.8	71.0	3.89	2.409(2), 2.357(2)	109.5(1)	4.09	[56a]
Group 12									
$[Hg(dppf)Cl_2]\cdot MeOH$	52.6	2.9	175.9	75.6	4.22	2.510(2), 2.516(2)	114.0(1)	4.03	[57]

[a] Two crystallographically independent molecules.
[b] Asymmetric unit defined by only half molecule.

Table 2
Relevant structural parameters for mononuclear complexes containing two η^2-chelating dppf ligands

Complex	τ (°)	Θ (°)	$X_A \cdots Fe \cdots X_B$ (°)	P···Fe···P (°)	P···P (Å)	M–P (Å)	P–M–P (°)	Fe···M (Å)	γ (°)	Ref.
Group 9										
$[Rh(dppf)_2]$	39.1, 18.5	2.9, 1.7	179.5, 179.1	64.2, 60.6	3.60, 3.48	2.306(1), 2.323(1), 2.312(1), 2.318(1)	102.2(1), 97.6(1)	4.32, 4.32	75.2	[58a]
$[Rh(dppf)_2][BF_4]\cdot 2\ C_2H_4Cl_2$	35.4, 24.1	7.5, 2.9	176.1, 178.3	60.9, 59.1	3.45, 3.39	2.312(3), 2.407(4), 2.358(3), 2.321(3)	94.0(1), 92.8(2)	4.45, 4.44	49.7	[59]
$[Na(THF)_5][Rh(dppf)_2]\cdot THF$	38.7, 21.2	2.7, 2.5	177.8, 179.1	62.9, 60.0	3.56, 3.45	2.230(5), 2.250(5), 2.244(5), 2.251(5)	105.1(2), 100.2(2)	4.27, 4.23	95.0	[58b]
$[Ir(dppf)_2]$	38.4, 18.7	4.4, 2.5	179.0, 178.9	63.3, 59.6	3.60, 3.47	2.296(3), 2.326(3), 2.301(4), 2.315(3)	102.1(1), 97.6(1)	4.37, 4.37	74.7	[60a]
$[Na(THF)_5][Ir(dppf)_2]\cdot THF$	38.0, 22.9	3.6, 3.4	177.8, 177.7	62.1, 59.6	3.56, 3.46	2.242(3), 2.256(3), 2.254(3), 2.270(3)	104.8(1), 99.8(1)	4.33, 4.28	95.0	[60b]
Group 11										
$[Ag(dppf)_2][ClO_4]\cdot 2\ CHCl_3$	59.9, 12.4	1.5, 7.4	177.9, 174.0	75.2, 67.7	4.10, 3.90	2.561(2), 2.585(2), 2.549(2), 2.601(2)	105.7(1), 98.4(1)	4.21, 4.26	88.3	[55c]

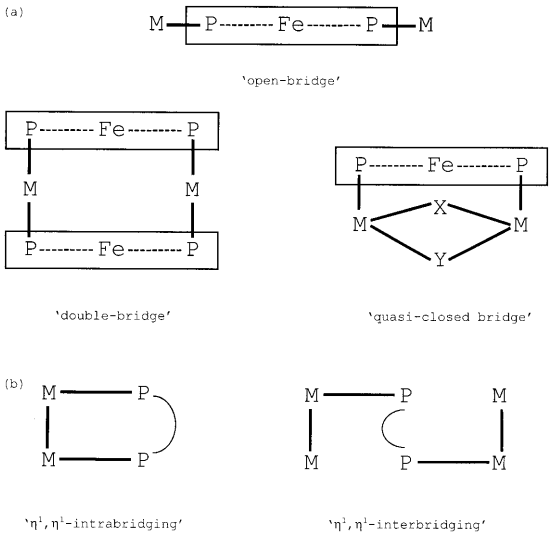

Scheme 1. (a) Coordinating modes of dppf; (b) binding modes in bimetallic complexes.

Fe–M bonding was found in the cluster $Ru_3(CO)_8(\mu\text{-H})[\mu_3\text{-}PPh_2(\eta^1,\eta^5\text{-}C_5H_3)Fe(\eta^5\text{-}C_5H_4)PPh_2]$ [16]. The latter is the only reported example of a formal dative bond from a ferrocenyl iron to a cluster core to date. On the contrary, there are rather frequent reports of dppf coordinating in the 'open-bridge' mode, where the dppf ligand bridges two M fragments [17] (Scheme 1a). The 'double bridge' mode and the 'quasi-closed bridge' one, as found in $Ag_2(\mu\text{-dppf})(\mu\text{-OOCPh})_2$ [18], are instead relatively rare in the literature. The binding modes found in bimetallic complexes are of two types: η^1,η^1-intrabridging (or closed bridge) and η^1,η^1-interbridging [6] (Scheme 1b).

3. Conformational modes of Cp rings

The dppf ligand versatility has been discussed in the previous section. The ability of the diphosphine to relieve the strain imposed by complex formation and to adjust its coordinating mode relies on the Cp rings mobility. The main motions involving the rings are (i) the torsional twist about the Cp(centroid)···Fe···Cp(centroid) axis and (ii) the tilt towards the Fe center or away from it. The twist is measured by the angle τ, which is the $C_A\cdots X_A\cdots X_B\cdots C_B$ torsion angle. C_A is the carbon atom of Cp ring 'A' bonded to the phosphorus atom; X_A is the Cp ring 'A' centroid. C_B and X_B indicate the same positions in Cp ring 'B'. Some geometrically regular dppf conformations in terms of the torsional twist angle τ are depicted in Fig. 3. The dppf ligand distortions can be estimated by the δ_P deviations (Å) of each linked phosphorus atom from the mean plane of the Cp ring to which the same atom belongs. This item will be discussed in Section 9. Although less

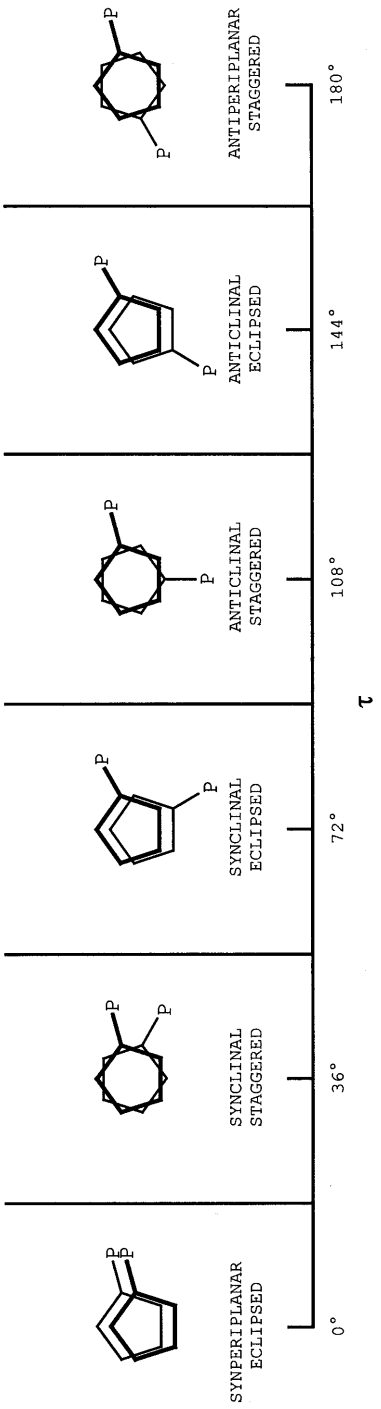

Fig. 3. Ideal conformations of dppf arising from Cp(centroid)···Fe···Cp(centroid) twist angle.

relevant, the mutual arrangement of the two Cp rings is measured by a third parameter (Θ), the dihedral angle between the mean planes through the Cp rings. These parameters and other metrical data describing the coordination geometry around the metal center have been calculated and reported for all the X-ray structures discussed (about 100).

4. Mononuclear complexes

In this investigation mononuclear complexes are the most populated group of structures (59 entries). Such a large collection can be conveniently divided into two subgroups. The first one gathers complexes showing a single η^2-chelating dppf and the second one collects structures showing two such ligands. The compounds belonging to each subgroup have then been further divided according to the Periodic Table Group to which the coordinated metal center belongs.

4.1. Mononuclear complexes containing a single η^2-chelating dppf

Table 1 reports the structurally characterized complexes, along with the relevant structural parameters relative to the dppf ligand and to the inner coordination

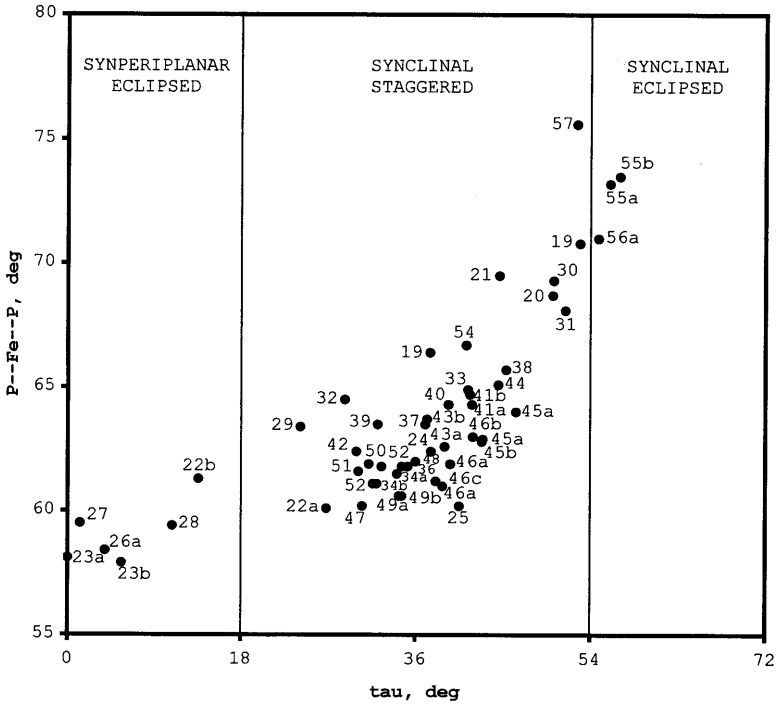

Fig. 4. P···Fe···P angle vs. torsion angle τ.

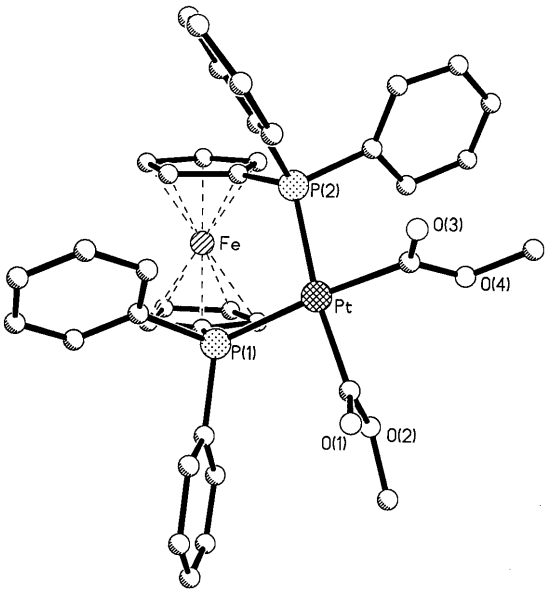

Fig. 5. Drawing of [Pt(dppf)(C(O)OMe)$_2$].

sphere about the metal (M) center. Some 83% of the examined structures shows dppf in the 'synclinal staggered' conformation, with the torsional twist τ angle confined between 18 and 54°. A plot of the ligand P···Fe···P separation versus the τ angle is depicted in Fig. 4. The graph shows that the synclinal staggered

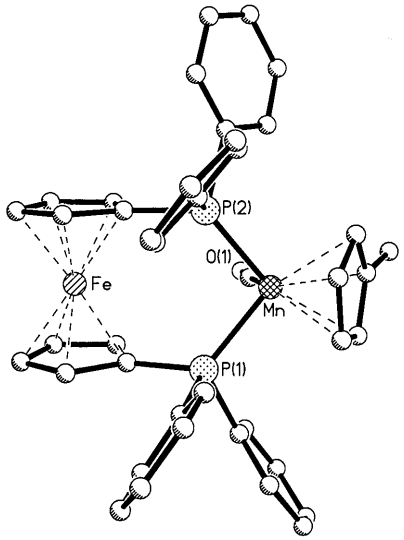

Fig. 6. Drawing of [Mn(dppf)(CO)(η^5-MeC$_5$H$_4$)].

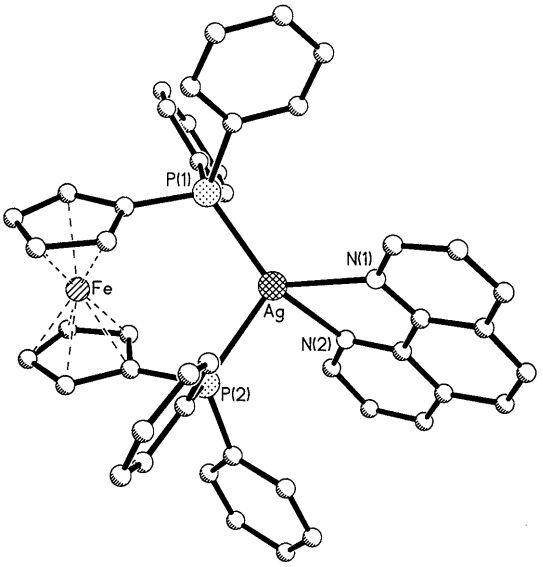

Fig. 7. Drawing of $[Ag(dppf)(phen)]^+$.

arrangement is largely preferred. Ideally, a synclinal staggered conformation has a τ angle of 36°. An arrangement close to this is shown by [Pt(dppf)(C(O)-OMe)$_2$]·MeOH [48] (Fig. 5). The perfect synperiplanar eclipsed conformation is shown instead by [Mn(dppf)(η^5-MeC$_5$H$_4$)]·CH$_2$Cl$_2$ [23a] (Fig. 6). Complex [Ag(dppf)(phen)][ClO$_4$] [55b] presents the largest τ value, 57.0° (Fig. 7).

Other interesting remarks are the following: (i) the Θ angle (the dihedral angle between the mean planes through the Cp rings) varies very little. In fact, Θ ranges between a minimum of 0.2° in [55a] and a maximum of 7.2° in [Ru(dppf)H(Cp*)] [25] and [Pt(dppf)(Me$_2$pz)$_2$] [46b]. (ii) The $X_A\cdots Fe\cdots X_B$ angle is always very close to 180°. The largest deviation (175.9°) is reported for [Hg(dppf)Cl$_2$]·MeOH [57]. (iii) The Fe···M separation varies between 4.03 Å in [57] and 4.55 Å in [Mo(dppf)(CO)$_4$] [19]; these numbers rule out the existence of a dative Fe→M interaction. (iv) The P–M–P angles range between 91.6(1)° in [Ru(dppf)(η^2-O$_2$)(Cp*)]$^+$ [28] (Fig. 8) and 114.0(1)° in [57] (Fig. 9).

Compound [28] is an example of a four-legged piano-stool structure, while compound [57] shows a distorted tetrahedral geometry. Actually, the P–M–P angle seems to be correlated with the number of the Periodic Table Group to which the coordinated metal center belongs. In fact, the P–M–P angle widens as the Group number increases. Thus, in the complexes containing a Group 10 metal the P–M–P angle ranges between 97.1(1) [46a] and 102.1(1)° [38], but in complexes with a Group 11 metal the same angle varies between 109.5(1) [56] and 112.9(1)° [53]. (v) A further correlation exists between the P···Fe···P and τ angles. The former is limited to within 57.9 [23b] and 75.6° [57]. The complex [Pd(dppf)(H$_2$norpcS$_2$)] [35,36] (Fig. 10) also deserves a mention. In this molecule the $[Pd(dppf)]^{2+}$ moiety

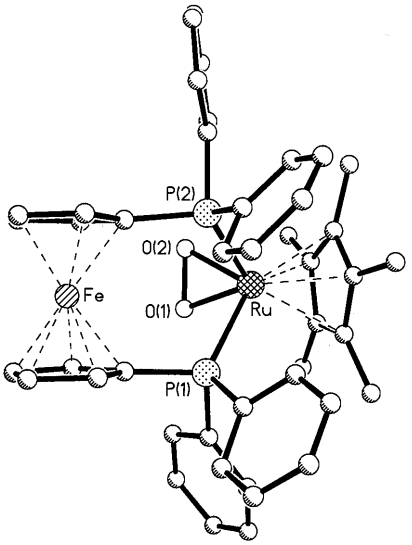

Fig. 8. Drawing of $[Ru(dppf)(\eta^2\text{-}O_2)(Cp^*)]^+$.

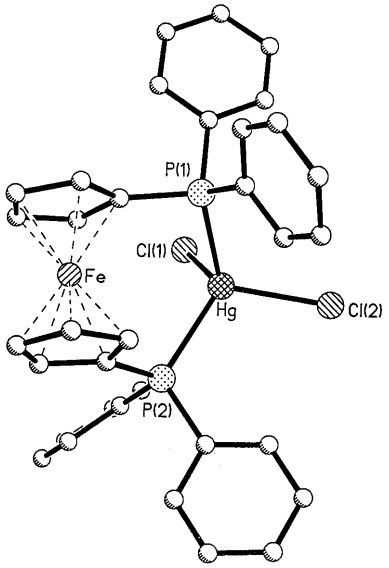

Fig. 9. Drawing of $[Hg(dppf)Cl_2]$.

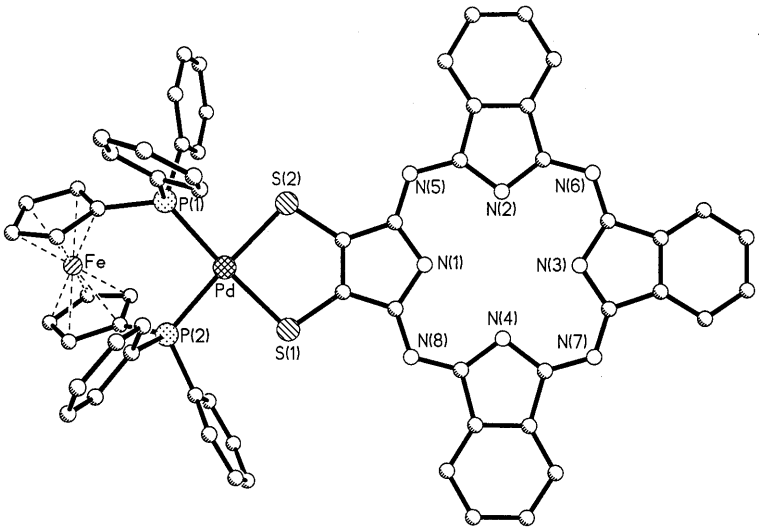

Fig. 10. Drawing of [Pd(dppf)(H_2norpcS_2)].

is coordinated to the peripheral dithiolate of the $(H_2norpcS_2)^{2-}$ core. The latter is an example of a macrocycle endowed with a peripheral metal-chelation site.

4.2. Mononuclear complexes containing two η^2-chelating dppfs

There are only six mononuclear complexes containing two chelating dppfs. In these structures the τ values appear to be very different (Table 2). The largest discrepancy is that found in $[Ag(dppf)_2]^+$ [55c], where the two τ values deviate by 47.5°. In this molecule both dppf ligands are unusually shaped, according to what has been discussed in Section 4.1. The two synthons take the synperiplanar eclipsed ($\tau = 12.4°$), and the synclinal eclipsed ($\tau = 59.9°$) arrangements, respectively (Fig. 11). In the remaining five structures the dppf ligands always appear in the synclinal staggered conformation. The three homoleptic rhodium complexes with the metal showing oxidation number 0, $+1$ and -1 attract special attention, and their structures are drawn in Fig. 12 ($[Rh(dppf)_2]^-$ [58b]), Fig. 13 ($[Rh(dppf)_2]$ [58a]) and Fig. 14 ($[Rh(dppf)_2]^+$ [59]).

In these compounds the coordination geometry around the metal center changes progressively. The shift is measured by the parameter γ (Table 2), that is, the dihedral angle defined by the P(1)–M–P(2) and the P(3)–M–P(4) planes, where P(1) and P(2) are the donor atoms of a dppf ligand, P(3) and P(4) those of the other. This measures how much the coordination around M deviates from an ideal tetrahedron ($\gamma = 90°$). In the three complexes the distortion becomes larger as the rhodium oxidation number increases from -1 to 0 and then to $+1$. Accordingly, γ shifts from 95.0 to 75.2 and then to 49.7°. At the same time, the angles about the rhodium atom approach 90°, the ideal value for square-planar coordination. A similar trend can be found in the corresponding Ir complexes, which are isostruc-

tural and isomorphous with the rhodium ones. The M–P distances of these complexes also deserve comment. As the complex charge falls from +1 to 0 and then from 0 to −1, the M–P distances first shorten ca. 0.04 Å, and then a further 0.05 Å. This phenomenon has been interpreted assuming that the M→P π bonding increases as the formal charge of the metal decreases.

5. Dinuclear complexes

In this section, 22 dinuclear structures are examined. The compounds have been divided in two groups, according to the coordinating mode of dppf. The first group (Table 3a) collects structures showing a η^2-chelating dppf ligand. The second one (Table 3b) gathers compounds where the synthon acts as a bridge. An examination of Table 3a reveals that the values of the structural parameters match those reported in Section 4.1, Table 1. However, the τ angles are restricted into a smaller domain ($31.7° \leq \tau \leq 45.1°$), so that τ is closer to the ideal synclinal staggered value (36°). The angle Θ too shows little variation, being limited between 1.0 and 4.5°, and the same can be said about the $X_A \cdots Fe \cdots X_B$ angle, which deviates from linearity only in the complex $[Ag_2(\mu\text{-dppf})(dppf)_2][PF_6]_2$ [63] (176.4°, Fig. 15). Also the P···P and the Fe···M separations do not change very much. The former ranges between 3.39 and 3.98 Å; the latter falls within 3.97 and 4.28 Å. By contrast, the M···M separation, which is as little as 3.07 Å in $[Pt_2(dppf)_2(thiaz)][BF_4]$ [50b] (Fig. 16), expands to 9.70 Å in $[Au_2(\mu\text{-dppf})(dppf)_2Cl_2]\cdot 2\ CH_2Cl_2$ [64] (Fig. 17).

This separation is particularly large in [63,64], $[Au_2(\mu\text{-dppf})(dppf)_2][ClO_4]_2\cdot 2\ CH_2Cl_2$ [56b], and $Au_2(\mu\text{-dppf})(dppf)_2][NO_3]_2\cdot 2\ H_2O$ [65]. These are 'open bridge'

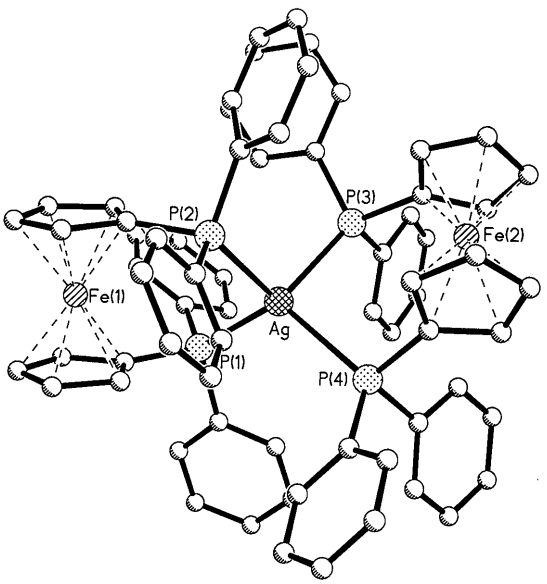

Fig. 11. Drawing of $[Ag(dppf)_2]^+$.

Table 3a
Relevant structural parameters for dinuclear complexes containing η^2-chelating dppf ligand/s

Complex	τ (°)	Θ (°)	$X_A \cdots Fe \cdots X_B$ (°)	P···Fe···P (°)	P···P (Å)	M–P (Å)	P–M–P (°)	Fe···M (Å)	M···M (Å)	Ref.
Group 10										
$[Pd_2(dppf)_2(\mu\text{-}Cl)_2][PF_6]_2$	33.3	3.7	178.5	61.3	3.39	2.278(2), 2.274(3)	96.4(1)	4.20	3.60	[61]
$[Pt_2(dppf)_2(thiaz)][BF_4]$	37.7, 35.3	2.8, 2.3	179.3, 178.4	63.5, 63.0	3.59, 3.56	2.342(6), 2.280(5) 2.286(6), 2.341(6)	101.9(2), 100.4(2)	4.24, 4.27	3.07	[50b][a]
Group 11										
$[Cu_2(dppf)_2(\mu\text{-}I)_2]\cdot 2\ CH_2Cl_2$	41.8	2.1	179.7	66.9	3.77	2.286(8), 2.28(1)	111.1(4)	4.04	3.53	[62a]
$[Cu_2(dppf)_2(\mu\text{-}ONO_2)_2]$	45.1	2.8	176.6	69.2	3.87	2.254(6), 2.262(6)	117.8(1)	3.97	3.43	[62b]
$[Cu_2(dppf)_2(\mu\text{-}O_2\text{–}CH\text{-}O,O')_2]$	37.6	1.0	178.3	65.9	3.72	2.276(1), 2.243(2)	110.8(1)	4.06	4.56	[62c]
$[Ag_2(\mu\text{-}dppf)(dppf)_2][PF_6]_2$	44.0	4.5	176.4	71.4	3.98	2.518(7), 2.481(7)	105.6(2)	4.15	9.32	[63]
$[Au_2(\mu\text{-}dppf)(dppf)_2Cl_2]\cdot 2\ CH_2Cl_2$	31.7	2.9	177.7	66.5	3.80	2.392(3), 2.405(3)	104.7(1)	4.28	9.70	[64]
$[Au_2(\mu\text{-}dppf)(dppf)_2][ClO_4]_2\cdot 2\ CH_2Cl_2$	42.4	1.2	177.4	69.2	3.87	2.378(3), 2.386(3)	108.8(1)	4.17	9.35	[56b]
$[Au_2(\mu\text{-}dppf)(dppf)_2][NO_3]_2\cdot 2\ H_2O$	43.3	3.5	177.2	69.6	3.90	2.396(3), 2.383(3)	109.2(1)	4.15	9.30	[65]

[a] With the exception of [50b], in these complexes the asymmetric unit is only half of the formula unit.

Table 3b
Relevant structural parameters for dinuclear complexes containing bridging dppf ligand/s

Complex	τ (°)	Θ (°)	$X_A\cdots Fe\cdots X_B$ (°)	P···Fe···P (°)	P···P (Å)	M–P (Å)	Fe···M (Å)	M···M (Å)	M–P···Fe (°)	α (°)	Φ (°)	Ref.
Group 6												
$[Mo_2(\mu\text{-dppf})(\mu\text{-pa})(CO)_6]\cdot 5/4\ Me_2CO$	118.4	1.1	178.1	125.5	6.13	2.588(3), 2.596(3)	4.82, 4.82	5.52	105.0, 104.8	121.1	77.4	[66]
Group 7												
$[Mn_2(\mu\text{-dppf})(\mu\text{-SPh})_2(CO)_6]\cdot 2\ CH_2Cl_2$[a]	71.6	7.5	173.9	96.1	5.27	2.390(6)	4.94	3.67	111.6	123.2	32.2	[67]
$[Re_2(\mu\text{-dppf})(\mu\text{-OH})_2(CO)_6]\cdot 5/2\ Me_2CO$	86.1	0.4	178.8	97.8	5.14	2.515(2), 2.531(2)	4.90, 4.93	3.42	111.1, 110.9	120.8	47.8	[68a]
$[Re_2(\mu\text{-dppf})(\mu\text{-OEt})_2(CO)_6]\cdot 1/2\ n\text{-hexane}$[a]	84.1	0.3	178.4	97.5	5.17	2.544(3)	4.96	3.43	111.2	123.3	52.9	[68b]
Group 8												
$[Fe_2(\mu\text{-dppf})(NO)_4Cl_2]$[a]	180.0	0.0	180.0	180.0	6.91	2.347(2)	4.69	9.38	106.4	110.6	70.6	[24b]
$[Ru_2(\mu\text{-dppf})(\eta^6\text{-}Me_4\text{–}C_6H_2)_2Cl_4]\cdot CH_2Cl_2$	118.6	4.1	175.6	131.2	6.43	2.350(4), 2.351(4)	5.11, 5.07	6.94	119.2, 117.9	113.3	60.4	[26b]
Group 10												
$[Pd_2(\mu\text{-dppf})(\text{arylamine})_2Br_2]\cdot CH_2Cl_2$[b]	143.4	2.6	176.4	154.0	4.24	2.269(2), 2.266(2)	4.46, 4.34	4.16	98.9, 95.3	116.3	82.8	[69]
	142.3	2.0	177.2	151.9	5.01	2.282(2), 2.273(2)	4.38, 4.46	4.95	96.2, 97.7	116.7	82.9	
Group 11												
$[Cu_2(\mu\text{-dppf})_2(\mu\text{-}\eta^1\text{-}C{\equiv}CC_6H_4Me\text{-}4)_2]$[c]	74.6	2.6	178.3	91.9	4.98	2.309(6), 2.316(7)	4.51, 4.47	2.45	100.6, 99.8	116.5	55.1	[70]
	79.9	1.4	179.2	91.2	4.90	2.283(7), 2.315(6)	4.51, 4.47		101.8, 101.0	117.1	58.5	
	77.7	0.4	178.8	91.4	4.90	2.305(6), 2.301(7)	4.47, 4.53	2.47	101.3, 102.2	117.3	58.8	
	74.8	1.2	179.1	92.1	5.02	2.313(6), 2.317(7)	4.48, 4.52		99.0, 100.5	116.2	55.8	
$[Ag_2(\mu\text{-dppf})_2(\mu\text{-Cl})_2]$	82.9	5.4	175.5	102.6	5.54	2.461(1), 2.474(1)	4.70, 4.85	3.46	102.5, 104.6	117.7	44.1	[71]
$[Ag_2(\mu\text{-dppf})(dppf)_2][PF_6]_2$[a]	180.0	0.0	180.0	180.0	6.91	2.457(6)	4.66	9.32	102.7	115.9	78.0	[63]
$[Au_2(\mu\text{-dppf})Cl_2]\cdot 2\ CH_2Cl_2$[a]	180.0	0.0	180.0	180.0	6.85	2.226(1)	4.30	8.60	96.7	112.8	81.6	[72a]
$[Au_2(\mu\text{-dppf})I_2]\cdot 2\ CH_2Cl_2$	170.2	2.1	179.1	175.3	6.87	2.248(9), 2.241(8)	4.29, 4.20	7.90	95.6, 92.8	111.3	83.2	[72b]
$[Au_2(\mu\text{-dppf})(dppf)_2Cl_2]\cdot 2\ CH_2Cl_2$[a]	180.0	0.0	180.0	180.0	7.04	2.345(3)	4.85	9.70	110.0	120.3	73.6	[64]
$[Au_2(\mu\text{-dppf})(dppf)_2][ClO_4]_2\cdot 2\ CH_2Cl_2$[a]	180.0	0.0	180.0	180.0	6.92	2.331(4)	4.67	9.35	106.0	116.3	75.3	[56]
$[Au_2(\mu\text{-dppf})(dppf)_2][NO_3]_2\cdot 2\ H_2O$[a]	180.0	0.0	180.0	180.0	6.93	2.337(3)	4.65	9.30	105.0	115.6	75.7	[65]
$[Au_2(\mu\text{-dppf})(\eta^1\text{-}OC(O)CF_3)_2]\cdot C_6H_{14}$[a]	180.0	0.0	180.0	180.0	6.94	2.217(2)	4.32	8.65	96.4	112.5	80.0	[73]
$[Au_2(\mu\text{-dppf})(\text{pyren-1-yl})_2]$[a]	180.0	0.0	180.0	180.0	6.92	2.295(2)	4.16	8.32	90.2	108.0	83.7	[74]

[a] Asymmetric unit defined by only half molecule.
[b] Two crystallographically independent molecules.
[c] Two whole molecules plus two half-molecules crystallographically independent.

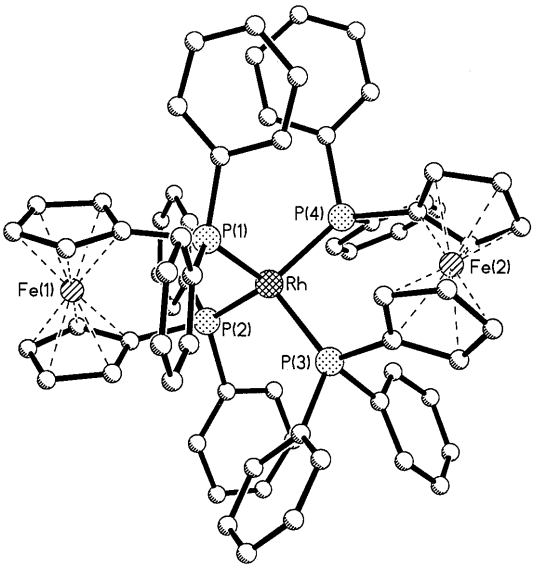

Fig. 12. Drawing of $[Rh(dppf)_2]^-$.

complexes, where a μ-bridging dppf acts as spacer between the two metal centers. Two additional structural parameters (α and Φ) have been introduced in Table 3b. They help to describe the dppf behavior when the latter behaves as a μ-bridging ligand. α is the average X···P–M angle; Φ is the angle formed by the projection of

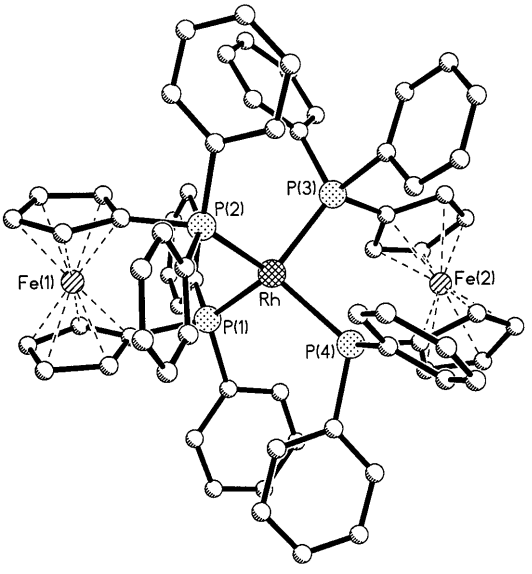

Fig. 13. Drawing of $[Rh(dppf)_2]$.

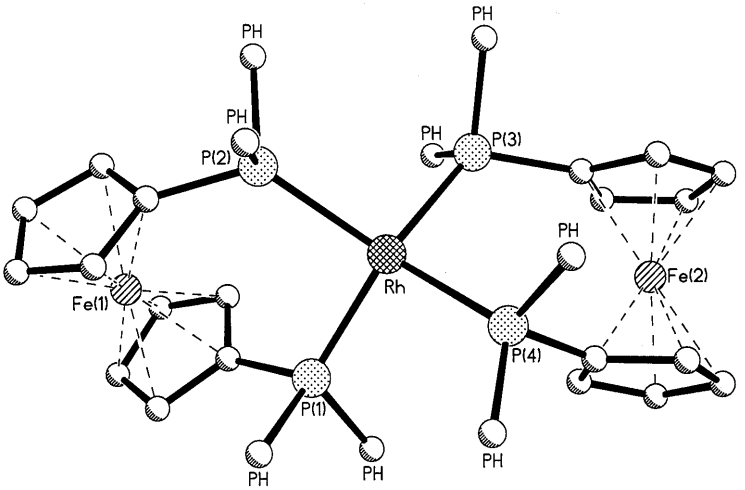

Fig. 14. Drawing of $[Rh(dppf)_2]^+$. PH denotes a phenyl ring.

the bridging dppf Cp···Cp axis onto the M···M vector. α varies between 108.0° in $[Au_2(\mu\text{-dppf})(\text{pyren-1-yl})_2]$ [74] (Fig. 18) and 123.2° in $[Mn_2(\mu\text{-dppf})(\mu\text{-SPh})_2(CO)_6]\cdot 2\,CH_2Cl_2$ [67] (Fig. 19).

Φ shows a larger variation, ranging from 32.2° in [67] to 83.7° in [74]. The angle Φ variability has already been noted in [68], and has been interpreted as 'sensitiveness'. That is, Φ seems to be the parameter better measuring the ability of dppf to 'fine-tune' its conformation in order to match the steric needs of the surrounding molecular environment. Interestingly, Φ values are larger ($> 70°$) when the μ-bridging dppf approaches an antiperiplanar staggered conformation ($\tau = 180°$). When

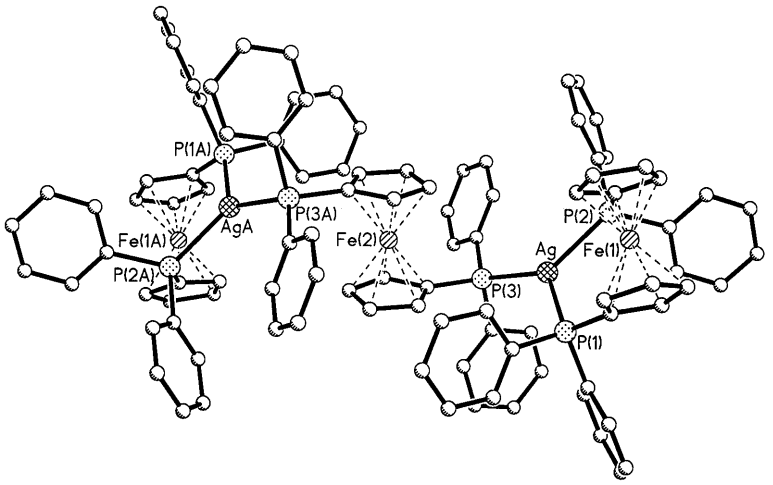

Fig. 15. Drawing of $[Ag_2(\mu\text{-dppf})(dppf)_2]^+$. Symmetrically related equivalent position for A is $\bar{x}$, $\bar{y}$, $\bar{z}$ ($\bar{1}$).

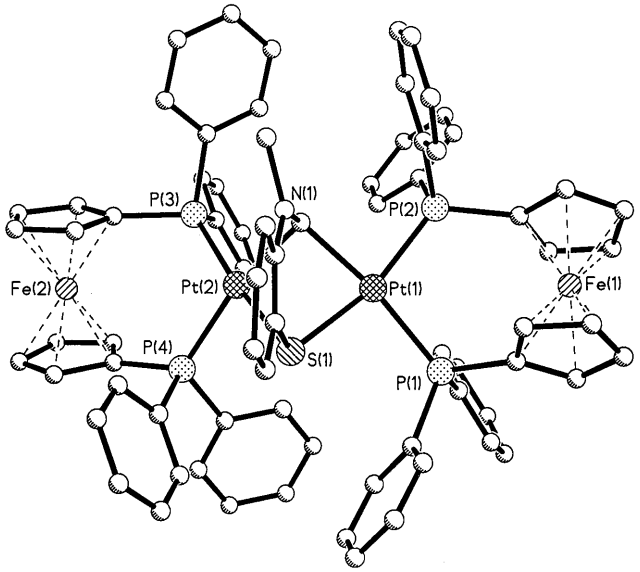

Fig. 16. Drawing of $[Pt_2(dppf)_2(thiaz)]^+$.

instead the dppf ligand has a synclinal eclipsed arrangement ($\tau = 72°$), Φ values are smaller (close to 50°).

6. Bimetallic M–M complexes

The six compounds belonging to this group are reported in Table 4. The complex $[Co_2(\eta^1\text{-dppf})(\mu_2\text{-}(MeO_2C)_2C_2)(CO)_5]$ [75] (Fig. 20) is the sole structure containing an η^1-coordinating dppf in the period covered by this review. The diphosphine ligand has an anticlinal eclipsed arrangement, with a τ angle of 154.9°. $[Pt_2(dppf)_2\text{-}(\mu\text{-H})(\mu\text{-pms})]Br\cdot 1/2\ CH_2Cl_2\cdot 1/2\ H_2O$ [76] (Fig. 21) is a dinuclear μ-alkylidene μ-hydride cation, where each dppf behaves as η^2-chelating and assumes a synclinal staggered conformation. The third molecule, $[Au_2(dppf)(\mu\text{-pdt})]$ [10] (Fig. 22), is a η^1,η^1-intrabridging complex, although it is questionable to affirm that the Au–Au separation in this molecule (3.060(1) Å) is a bond.

The three structures $[Au_2(\mu\text{-dppf})(\mu\text{-S})]\cdot 2\ CHCl_3$ [77], $[Au_3(\mu\text{-dppf})(\mu_3\text{-S})(C_6F_5)_3]$ [78] and $[Au_4(\mu\text{-dppf})(\mu_4\text{-S})(C_6F_5)_6]\cdot 2\ CH_2Cl_2$ [79] look very similar and are presented together. The last two might have been discussed in the next section, but we have decided to give priority to the dppf binding mode. In fact, in these structures the diphosphine always acts as a μ-bridging ligand, so that these all are η^1,η^1-intrabridging complexes. The similarity is emphasized by examining the values of the parameters describing the behavior of dppf reported in Table 4, among which is the ε parameter. The latter is the smaller of the two P–M–M–P dihedral angles. In the last three structures dppf has a synclinal eclipsed arrangement, and all metrical data

Table 4
Relevant structural parameters for bimetallic M–M complexes containing dppf ligand/s

Complex	τ (°)	Θ (°)	$X_A\cdots Fe\cdots X_B$ (°)	P···Fe···P (°)	P···P (Å)	M–P (Å)	M–M (Å)	P···M···P (°)	Fe···M (Å)	ε (°)	Ref.
Group 9											
$[Co_2(\eta^1\text{-dppf})(\mu_2\text{-}(MeO_2C)_2C_2)(CO)_5]$	154.9	1.3	178.1	156.9	6.78	2.224(1)	2.474(1)		4.75		[75]
Group 10											
$[Pt_2(dppf)_2(\mu\text{-H})(\mu\text{-pms})]Br\cdot 1/2\ CH_2Cl_2\cdot 1/2\ H_2O$	38.3, 33.6	2.4, 0.8	178.7, 179.0	63.4, 63.2	3.52, 3.56	2.245(2), 2.334(2), 2.258(2), 2.310(2)	2.731(1)	100.6, 102.2	4.18, 4.24	11.3, 3.3	[76]
Group 11											
$[Au_2(dppf)(\mu\text{-pdt})]$	62.7	4.1	174.6	87.8	4.84	2.266(3), 2.267(3)	3.060(1)	90.8, 92.3	4.55, 4.60	70.1	[10]
$[Au_2(\mu\text{-dppf})(\mu\text{-S})]\cdot 2\ CHCl_3$[a]	86.1	6.2	174.3	101.7	5.31	2.246(2)	2.883(1)	97.9	4.30	2.7	[77]
$[Au_3(\mu\text{-dppf})(\mu_3\text{-S})(C_6F_5)_3]$	84.6	3.8	175.7	100.9	5.31	2.245(3), 2.245(4)	2.888(1)	99.0, 96.9	4.30, 4.36	2.0	[78]
$[Au_4(\mu\text{-dppf})(\mu_4\text{-S})(C_6F_5)_6]\cdot 2\ CH_2Cl_2$	87.3	4.5	175.1	102.4	5.32	2.255(3), 2.252(3)	2.956(1)	95.5, 97.9	4.35, 4.28	3.1	[79]

[a] The molecule has crystallographic twofold symmetry.

are equal within experimental error. Fig. 23 shows a perspective view of complex [77].

7. Trinuclear and tetranuclear complexes containing dppf

In the 1994–98 period, only five trinuclear and two tetranuclear dppf containing complexes have been structurally characterized. These compounds are reported in Table 5. Here, the subdivision according to the Periodic Table Group has been dropped, as it would have been meaningless in the case of heteronuclear compounds. However, Table 5 does not look heterogeneous as, with the sole exception of $[Au_3(\mu\text{-dppf})(\mu_3\text{-Spy})(PPh_2Me)][OTf]_2\cdot C_2H_4Cl_2$ [72c], all reported structures contain Group 10 metals. In these molecules dppf acts mainly as an η^2-chelating ligand, sometimes as a bridge. Interestingly, only one complex shows dppf in both modes, that is $[Pd_3(\mu\text{-dppf})(dppf)(\mu_3\text{-S})_2Cl_2]\cdot 2\ CH_2Cl_2$, [80a] (Fig. 24).

Accordingly, the parameters in Table 5 show rather large variations, although the values do not differ from those seen previously (Tables 1 and 3b). All the complexes where the diphosphine ligand coordinates in η^2-chelating mode show dppf in a synclinal staggered arrangement. In the same way, when dppf behaves as a μ-ligand, τ values match those reported in Table 3b. In the tetranuclear complex $[Pd_2Os_2(\mu\text{-dppf})(\mu\text{-I})_4(CO)_4I_4]\cdot CH_2Cl_2$ [82], the torsional twist angle value is close to that of an ideal anticlinal eclipsed conformation. It is worth noting that the only other Pd-containing structure showing this arrangement is $[Pd_2(\mu\text{-dppf})\text{-}(arylamine)_2Br_2]\cdot CH_2Cl_2$ [69] (Table 3b). As usual, the Θ value is slightly greater than 0°, and ranges from 1.9° in $[Pd_2Ag_2(dppf)_2(\mu_3\text{-S})_2Cl_2]\cdot 4\ CH_2Cl_2$ [83] (Fig. 25) to 6.0° in [80a].

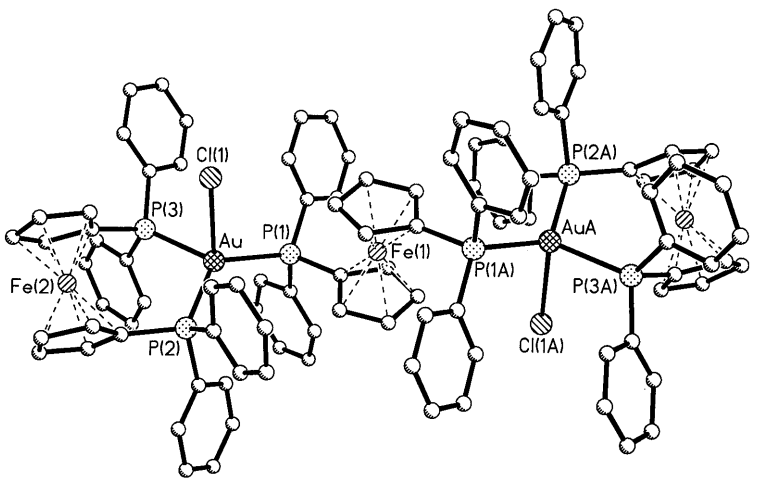

Fig. 17. Drawing of $[Au_2(\mu\text{-dppf})(dppf)_2Cl_2]$. Symmetrically related equivalent position for A is $\bar{x}$, $\bar{y}$, $\bar{z}$ ($\bar{1}$).

Table 5
Relevant structural parameters for trinuclear and tetranuclear complexes containing dppf ligand/s

Complex	τ (°)	Θ (°)	$X_A \cdots Fe \cdots X_B$ (°)	P···Fe···P (°)	P···P (Å)	M–P (Å)	P···M···P (°)	Fe···M (Å)	M···M (Å)	α (°)	Ref.
$[Pd_3(\mu\text{-dppf})(dppf)(\mu_3\text{-}S)_2Cl_2]\cdot 2\ CH_2Cl_2$	35.8, 75.9	1.5, 6.0	178.1, 174.0	63.6, 98.7	3.57, 5.38	2.316(1), 2.323(1), 2.294(2), 2.284(1)	100.8, 92.2, 96.7	4.26, 4.64, 4.44	3.13, 3.12, 3.13	109.6, 121.2	[80a]
$[Pd_3(dppf)_2(\mu_3\text{-}S)_2(PPh_3)Cl]Cl$	39.5, 37.1	4.1, 4.1	178.6, 179.6	63.4, 63.6	3.57, 3.60	2.309(2), 2.322(2), 2.321(2), 2.324(2)	101.0, 101.7	4.23, 4.31	3.20		[80b]
$[Pd_3(dppf)_2(\mu_3\text{-}S)_2(PPh_3)Cl]\ [NO_3]\cdot CH_2Cl_2$	40.5, 37.1	4.1, 3.3	177.5, 179.5	63.0, 63.6	3.52, 3.58	2.334(2), 2.318(2), 2.333(2), 2.326(2)	98.4, 100.4	4.18, 4.32	3.24		[80c]
$[Pt_2Tl(dppf)_2(\mu_3\text{-}S)_2][PF_6]$[a]	36.4	4.9	178.4	61.1	3.44	2.285(2), 2.293(2)	97.5	4.26	3.28		[81]
$[Au_3(\mu\text{-dppf})(\mu_3\text{-Spy})(PPh_2Me)][OTf]_2\cdot C_2H_4Cl_2$	89.7	2.5	176.8	102.7	5.28	2.246(4), 2.238(5)	97.3, 94.1	4.17, 4.34	3.21, 3.10	114.5, 115.5	[72c]
$[Pd_2Os_2(\mu\text{-dppf})_2(\mu\text{-}I)_4(CO)_4I_4]\cdot CH_2Cl_2$[a]	142.3	2.7	175.4	150.9	6.85	2.288(8), 2.367(9)	151.9, 116.0	4.35, 5.49	3.91, 4.11	108.0, 119.2	[82]
$[Pd_2Ag_2(dppf)_2(\mu_3\text{-}S)_2Cl_2]\cdot 4\ CH_2Cl_2$[a]	40.1	1.9	179.3	62.9	3.53	2.334(1), 2.340(1)	98.0	4.24	3.56		[83]

[a] Asymmetric unit made by only half molecule.

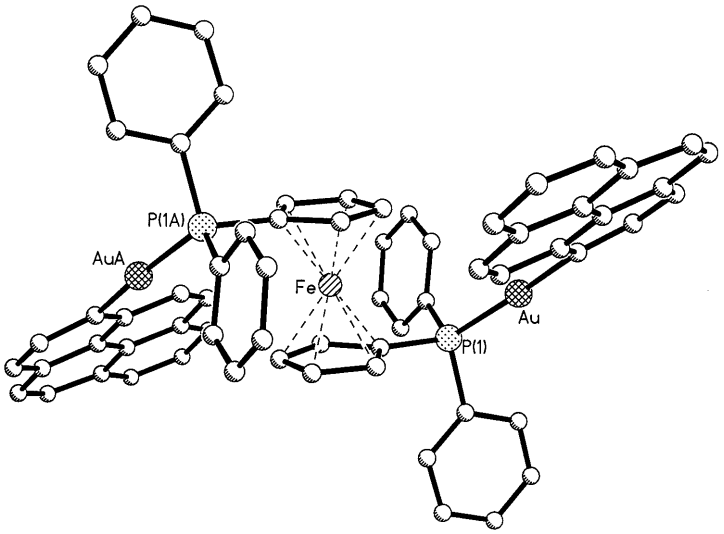

Fig. 18. Drawing of $[Au_2(\mu\text{-dppf})(\text{pyren-1-yl})_2]$. Symmetrically related equivalent position for A is $\bar{x}$, $\bar{y}$, $\bar{z}$ ($\bar{1}$).

Similarly, also the $X_A\cdots Fe\cdots X_B$ angle does not vary significantly. The largest deviation from 180° is again found in [80a]. The P···M···P angle ranges from 92.2 in [80a] to 151.9° in [82]; the latter, however, is an improper P···M···P angle. In fact,

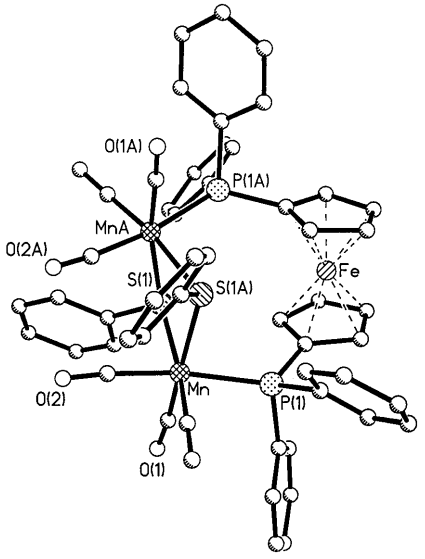

Fig. 19. Drawing of $[Mn_2(\mu\text{-dppf})(\mu\text{-SPh})_2(CO)_6]$. Symmetrically related equivalent position for A is $1/2 + x$, $\bar{y}$, z (plane a).

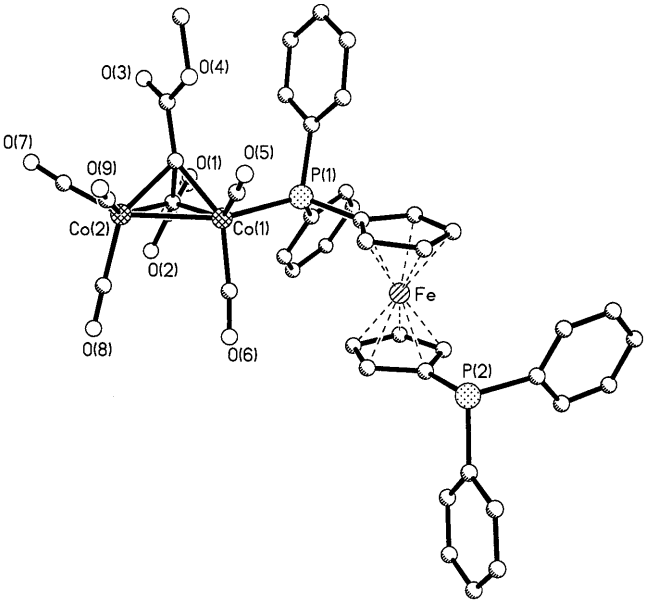

Fig. 20. Drawing of $[Co_2(\eta^1\text{-dppf})(\mu_2\text{-}(MeO_2C)_2C_2)(CO)_5]$.

the dppf ligands in this complex act only as a bridge, and we measured the P···M···P angle by picking the phosphorus atom of a dppf unit, the metal atom bonded to it, and the closest phosphorus atom of the second dppf unit. The P···P separations and the α angles are in agreement with those found in mono- and dinuclear complexes. There is no evidence of metal–metal bonds or of $Fe \rightarrow M$ interactions in these structures. The M···M distance varies between 3.10 in [72c] and 4.11 Å in [82]; the Fe···M separation remains within 4.17 Å, again in [72c], and 5.49 Å in [82]. The tripalladium complexes described in [80] ($[Pd_3(\mu\text{-dppf})(dppf)(\mu_3\text{-}S)_2Cl_2]\cdot 2\ CH_2Cl_2$, $[Pd_3(dppf)_2(\mu_3\text{-}S)_2(PPh_3)Cl]Cl$ and $[Pd_3(dppf)_2(\mu_3\text{-}S)_2(PPh_3)Cl][NO_3]\cdot CH_2Cl_2$), the tetranuclear complex shown in [83] and the complex $[Pt_2Tl(dppf)_2(\mu_3\text{-}S)_2][PF_6]$ [81] deserve particular mention. The structures described in [80,81] present an M_3S_2 core shaped in an intriguing 'Mexican-hat-like' arrangement, as it has been imaginatively defined by Hor and coworkers [81]. The M_3S_2 core can be obtained through metallation of a M_2S_2 nucleus, like the one of $[Pd_2Ag_2(dppf)_2(\mu_3\text{-}S)_2Cl_2]$ [83]. In one of these compounds [80a] the dppf ligand exhibits fluxional behavior, despite its large steric bulk. The situation seems favored by the stability imposed on the M_3S_2 core by the triply bridging sulfides. This allows the cooperative rearrangement of the two dppfs on the M_3 triangle.

8. Addenda

During the preparation of this review three more X-ray structures have been published: [Rh(dppf)(Cp*)Cl][PF_6], [Rh(dppf)(Cp*)(*p*-TosCH_2NC)][PF_6] and [Rh(μ-dppf)(Cp*)$_2$$Cl_2$] [84]. These compounds are briefly outlined in this section. All these arene–Rh(III) complexes show the 'piano-stool' structure around the metal. In the first two members of the series the dppf synthon acts as an η^2-chelating agent, showing a synperiplanar conformation; the P···P separation is of ca. 3.5 Å. The third complex is instead another example of a dimeric structure bridged by a dppf ligand. In this molecule the two rings assume an anticlinal eclipsed conformation and the P···P separation rises to 6.84 Å. Recently, Butler and coworkers [85] have announced the synthesis and characterization of 1,3-bis-(diphenylphosphino)ferrocene. This molecule is a putative ligand towards a new area of ferrocene–ligand chemistry, offering exciting opportunities in catalysis.

9. Conclusions

The goal of this review was to investigate the coordination ability exhibited by the dppf ligand. About 100 structures have been considered and the dppf coordinating modes accurately examined. Only four such modes have been found. The η^2-chelating mode largely dominates over the μ-bridging one; four bimetallic complexes adopt the η^1,η^1-intrabridging mode and only one structure shows η^1-unidentate dppf. The flexibility of the diphosphine ligand has been evaluated

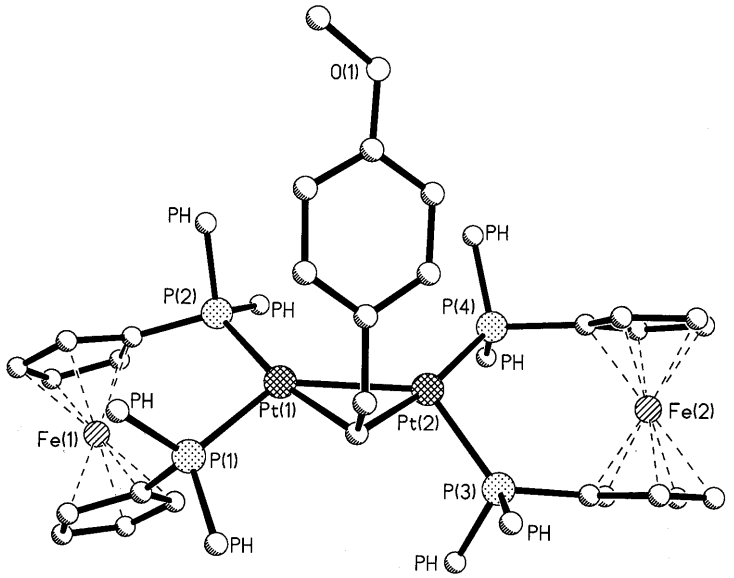

Fig. 21. Drawing of [Pt_2(dppf)$_2$(μ-H)(μ-pms)]$^+$. PH denotes a phenyl ring.

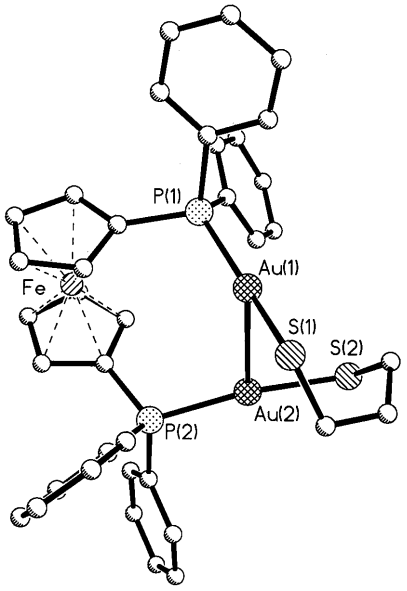

Fig. 22. Drawing of $[Au_2(dppf)(\mu\text{-}pdt)]$.

with a series of parameters involving physical (specific atoms) and geometrical (centroids) entities.

The calculated data indicate a rigid-body motion of the ferrocene moiety. In fact, neither the $X_A\cdots Fe\cdots X_B$ angle nor the Θ angle deviate significantly from their ideal values of 180 and 0°, respectively. Interestingly, both parameters show their largest shifts in complex $[Mn_2(\mu\text{-}dppf)(\mu\text{-}SPh)_2(CO)_6]\cdot 2\ CH_2Cl_2$ [67] (Fig. 19), where the $X_A\cdots Fe\cdots X_B$ angle goes to 173.9° and the Θ angle reaches 7.5°. A Θ value of 7.5° is found also in $[Rh(dppf)_2][BF_4]\cdot 2\ C_2H_4Cl_2$ [59]. Probably, the shifts from ideal values in [67] are due to the rigidity of the Mn_2S_2 core that forces the ferrocene moiety to lose its preferential arrangement. This would suggest that the dppf synthon matches the needs of its molecular environment by changing the mutual positions of the phosphorus atoms.

The torsional twist τ angle measures this motion. Although in the calculated data τ varies from 0 to 180°, not all dppf arrangements arising from the twist are equally populated. Actually, only 13 of the structures investigated show a τ angle greater than 90°, and not one adopts the anticlinal staggered conformation. The synclinal staggered arrangement is largely preferred and is found in more than 70% of structures. The staggered arrangement of the Cp rings is also preferred in a broader sense. In fact, by also taking into account the structures where dppf has an antiperiplanar staggered conformation, there are 73 complexes (81%) containing staggered dppf ligands.

Even if the τ variation is the main path through which dppf meets the demands of the molecular environment, other motions of the phosphorus atoms are involved.

The P···Fe···P, P···P, P–M–P and δ_P parameters measure these motions; all such metrical data are correlated to τ. The best correlation exists between the τ and P···Fe···P angles (Section 4.1, Fig. 4), but similar relations hold also for the P···P and the P–M–P parameters. However, the trend can best be appreciated in complexes containing η^2-chelating dppf. The P···Fe···P angle in complexes showing η^2-chelating dppf ligands spans a domain of nearly 18°, ranging between 57.9° in $[Mn(dppf)(CO)(\eta^5\text{-}MeC_5H_4)]\cdot CH_2Cl_2$ (isomer ii) [23b] (Fig. 6) and 75.6° $[Hg(dppf)Cl_2]\cdot MeOH$ [57] (Fig. 9). The variation of this parameter in complexes with μ-bridging dppf ligands approaches 90°, as the P···Fe···P angle extends from 91.2° in $[Cu_2(\mu\text{-}dppf)_2(\mu\text{-}\eta^1\text{-}C{\equiv}CC_6H_4Me\text{-}4)_2]$ [70] to 180° (crystallographically imposed) in various complexes. The value reported in the η^1,η^1-intrabridging bimetallic complex $[Au_2(dppf)(\mu\text{-}pdt)]$ [10] (Fig. 22) is 87.8°.

The P···P separation in compounds bearing η^2-chelating diphosphines is restricted between 3.36 Å in [23b] and 4.22 Å in [57] (notably, the same compounds as before), thus varying over 0.9 Å. As above, complexes containing μ-bridging ligands show a larger variation. The domain spanned is 2.80 Å and ranges from 4.24 Å in $[Pd_2(\mu\text{-}dppf)(arylamine)_2Br_2]\cdot CH_2Cl_2$ [69] and 7.04 Å in $[Au_2(\mu\text{-}dppf)(dppf)_2Cl_2]\cdot 2\ CH_2Cl_2$ [64] (Fig. 17) (Table 3b). The η^1,η^1-intrabridging compound [10] shows a value of 4.84 Å. It is worth noting, however, that these are *nonbonding* distances. The P–M–P bonding angle ranges instead from 92.0(1)° in $[Ru(dppf)(\eta^6\text{-}Me_6C_6)Cl][PF_6]$ [26a] to a strikingly large 117.8(1)° in $[Cu_2(dppf)_2$-

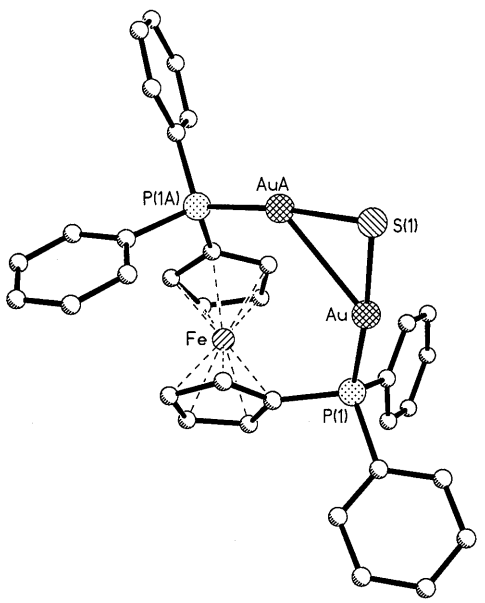

Fig. 23. Drawing of $[Au_2(\mu\text{-}dppf)(\mu\text{-}S)]$. Symmetrically related equivalent position for A is $1/2-x$, y, $1/2-z$ (plane n).

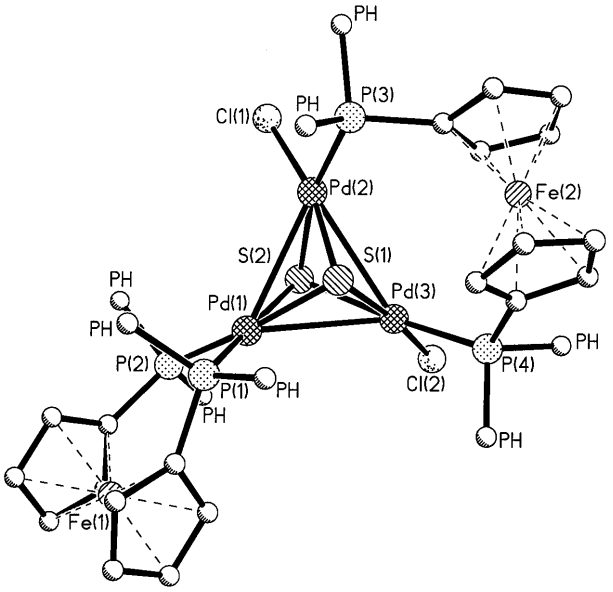

Fig. 24. Drawing of $[Pd_3(\mu\text{-dppf})(dppf)(\mu_3\text{-}S)_2Cl_2]$. PH denotes a phenyl ring.

$(\mu\text{-}ONO_2)_2]$ [62b]. The latter represents the largest ever reported for dppf chelates of any metal in all geometries. The planarity of the Cu_2O_2 core and of the ONO_2 entity is probably the most important contribution to the large bite angle.

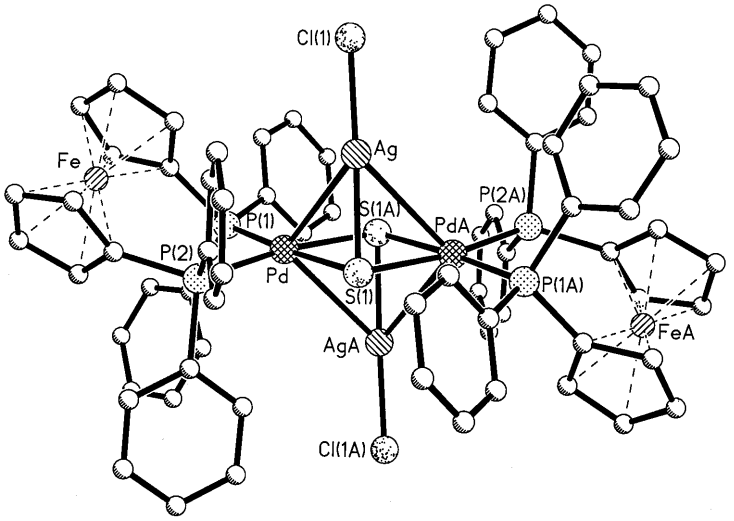

Fig. 25. Drawing of $[Pd_2Ag_2(dppf)_2(\mu_3\text{-}S)_2Cl_2]$. Symmetrically related equivalent position for A is $\bar{x}$, $\bar{y}$, $\bar{z}$ $(\bar{1})$.

All these data confirm that dppf versatility hinges on the motion of the phosphorus atoms. The ability to achieve metal coordination is also sustained by the opportunity of displacing the phosphorus atoms away from the Cp ring to which they belong. The displacement is measured by the δ_P deviations, as has been pointed out in Section 3 when discussing the distortions of the dppf ligands. δ_P deviations normally do not exceed ± 0.10 Å; a positive sign means that the phosphorus atoms lies on the same side of the Cp ring as the iron atom. However, δ_P displacements are sometimes bigger. This happens with the cationic complexes $[Ru(dppf)(\eta^6\text{-}Me_6C_6)Cl]^+$ [26a], $[Ru(dppf)(\eta^6\text{-}p\text{-cymene})Cl]^+$ [27], $[Ru(dppf)(bipy)_2]^{2+}$ [29] and $[Ag(dppf)_2]^+$ [55c] (Fig. 11). δ_P deviations in these structures are, respectively: -0.124, -0.177; -0.067, -0.186; -0.151, -0.151; 0.005, -0.191. The shifts become very noticeable in the complexes $[Pd_2(\mu\text{-dppf})(arylamine)_2Br_2]\cdot CH_2Cl_2$ [69] and $[Ag_2(\mu\text{-dppf})_2(\mu\text{-Cl})_2]$ [71]. In the former there are two independent molecules in the asymmetric unit and δ_P deviations are -0.194, -0.189; -0.176, -0.225; in the latter they assume the values of -0.136, -0.350.

With respect to M–P distances, it is difficult to discuss trends for all metals. Actually, only palladium, platinum, copper, silver, gold and, perhaps, ruthenium compounds appear to be sufficiently represented (Fig. 2b). Thus, a brief discussion will only be made about these structures. In Pd complexes the shortest Pd–P distance is 2.262(4) Å in $[Pd(dppf)Cl_2]\cdot CH_2Cl_2$ [34a]; the longest one is 2.401(2) Å in [Pd(dppf)Br(clan)] [37]. The spread is 0.14 Å. The corresponding values in Pt structures are, respectively, 2.219(3) Å in $[Pt(dppf)(O_2CPh)_2]\cdot CH_2Cl_2$ [49b] and 2.354(1) Å in $[Pt(dppf)(thiaz)][BF_4]$ [50a] (Fig. 16). The range covered is again 0.14 Å, and this equivalency highlights the similarity between the two metals.

Compounds of Group 11 show a more complex behavior. M–P distances increase when moving from Cu to Ag structures and shorten when passing from Ag to Au complexes. The smallest M–P distances found for Cu, Ag, Au are, respectively, 2.243(2) Å in $[Cu_2(dppf)_2(\mu\text{-}O_2\text{-}CH\text{-}O,O')_2]$ [62c], 2.411(1) Å in [Ag(dppf)(phen)][ClO_4] [55b] (Fig. 6) and 2.217(2) Å in $[Au_2(\mu\text{-dppf})(\eta^1\text{-}OC(O)CF_3)_2]\cdot C_6H_{14}$ [73]. The biggest M–P distances for the same metal centers are 2.317(7) Å in $[Cu_2(\mu\text{-dppf})_2(\mu\text{-}\eta^1\text{-}C{\equiv}CC_6H_4Me\text{-}4)_2]$ [70], 2.601(2) Å in $[Ag(dppf)_2][ClO_4]\cdot 2\ CHCl_3$ [55c] and 2.409(2) Å in $[Au(dppf)(PPh_3)][ClO_4]\cdot CHCl_3$ [56a]. The covered range is 0.07 Å for copper, 0.19 Å for silver and 0.19 Å for gold. A similar evaluation for the seven-membered series of ruthenium complexes reported in Table 1 reveals that Ru–P distances span an even larger domain. The smallest Ru–P bond measures 2.259(1) Å in [Ru(dppf)H(Cp*)] [25]; the biggest one is 2.518(4) Å in $[Ru(dppf)(CO)(PPh_3)ClH]$ [30]. The bond distance range in these compounds is 0.26 Å.

The Fe···M separations also deserve a brief mention. The shortest separation is 3.97 Å in $[Cu_2(dppf)_2(\mu\text{-}ONO_2)_2]$ [62b], a complex whose peculiarity has been discussed previously. The largest separation, 5.49 Å, is found instead in the μ-bridging dppf ligand of $[Pd_2Os_2(\mu\text{-dppf})_2(\mu\text{-}I)_4(CO)_4I_4]\cdot CH_2Cl_2$ [82]. In any case, the separations are too big for a direct Fe–M interaction. The catalytic activity of dppf complexes can then be played only through the phosphorus atoms and such

a conclusion reinforces the concept of the central role of phosphorus atoms in determining dppf properties.

Some comments can finally be made about the coordination geometry around the metal centers of the structures examined. Also this discussion will be limited to complexes containing Group 10 or 11 metals, because there are a representative number of structures from which useful conclusions may be made (Fig. 2b). The following points can be made.

1. In all palladium complexes the metal has a +2 oxidation state and a square-planar environment which occasionally shows some distortion. The distortion can be appreciated by examining how significantly the angles around the metal deviate from 360°, or by measuring the dihedral angle γ formed by the P–Pd–P and L–Pd–L planes (L = donor atom). The biggest deviations from ideal square-planar coordination are found in [Pd(dppf)($C_{18}H_{24}O_8$)]·Me_2CO (one enantiomer) [41a] and [Pd(dppf)($C_{18}H_{24}O_8$)] (racemate) [41b]. In the former, the sum of the angles about Pd reaches 368.1° and $\gamma = 30.4°$; in the latter, the same values are 366.9° and 28.4°, respectively. The greatest 'bite' angle, 102.1(1)°, belongs to complex [Pd(dppf)Br(η^1-C_5H_4NH-C^2)]Br·1/2 MeOH [38]; the smallest, 97.8(2)°, to complex [Pd(dppf)Cl_2]·CH_2Cl_2 [34a].
2. All platinum complexes too have the metal in the +2 oxidation state and a square-planar geometry, with the exception of the structures described in [44] and [50b]. The structure that deviates more from the ideal arrangement is [Pt(dppf)(bph)]·2 CH_2Cl_2 [45b]. In the latter, the sum of the angles around Pt reaches 362.8° and $\gamma = 18.4°$. The 'bite' angle ranges from 97.3(2)° in [Pt(dppf)(C(O)OMe)$_2$)]·MeOH [48] (Fig. 15) to 101.5(3)° in [Pt(dppf)(Me_2pz)$_2$] [46b]. The compounds described in [44,50a] are both Pt(0) complexes. In [Pt(dppf)(*trans*-stilbene)]·THF [44] the coordination geometry is trigonal and almost planar; the angles about platinum add to 360.6°, with $\gamma = 11.5°$. In [Pt(dppf)(thiaz)][BF_4] [50a] (Fig. 16) the metal shows a square planar arrangement, the angles at Pt sum 362.5° and $\gamma = 19.1°$.
3. All Group 11 complexes show the metal in the +1 oxidation state. Interestingly, many of these structures (Table 3b) show both chelating and bridging dppf ligands. The coordination geometry around copper(I) is always distorted tetrahedral, while the situation is different in silver(I) complexes. The geometry around silver is trigonal in [Ag(dppf)(PPh_3)][ClO_4]·2 CH_2Cl_2 [55a] and [Ag_2(μ-dppf)(dppf)$_2$][PF_6]$_2$ [63] (Fig. 15). A tetrahedral environment is found instead in [Ag(dppf)$_2$][ClO_4]·2 $CHCl_3$ [55c] (Fig. 11) and [Ag_2(μ-dppf)$_2$(μ-Cl)$_2$] [71]. The deviation from an ideal tetrahedral arrangement is especially clear in [Cu_2-(μ-dppf)$_2$(μ-η^1-C≡CC_6H_4Me-4)$_2$] [70], where $\gamma = 78.2°$ and the P–Cu–P angle opens to till 118.9(3)°. In compound [71] the P–Ag–P angle gets to 129.9(4)°, but the environment around silver shapes in a nearly regular tetrahedron ($\gamma = 88.8°$).The geometry found in gold complexes is of two types: trigonal or linear. [Au(dppf)(PPh_3)][ClO_4]·$CHCl_3$ [56a], [Au_2(μ-dppf)(dppf)$_2$][ClO_4]$_2$·2 CH_2Cl_2 [56b], [Au_2(μ-dppf)(dppf)$_2Cl_2$]·2 CH_2Cl_2 [64] (Fig. 17) and [Au_2(μ-dppf)(dppf)$_2$][NO_3]$_2$·2 H_2O [65] all have a trigonal environment. A linear coordination is shown by [Au_2(μ-dppf)Cl_2]·2 CH_2Cl_2 [72a], [Au_2(μ-dppf)I_2]·2 CH_2Cl_2

[72b], $[Au_3(\mu\text{-dppf})(\mu_3\text{-Spy})(PPh_2Me)][OTf]_2\cdot C_2H_4Cl_2$ [72c], $[Au_2(\mu\text{-dppf})(\eta^1\text{-}OC(O)CF_3)_2]\cdot C_6H_{14}$ [73], $[Au_2(\mu\text{-dppf})(\text{pyren-1-yl})_2]$ [74] (Fig. 18), $[Au_2(\text{dppf})(\mu\text{-pdt})]$ [10] (Fig. 22) and $[Au_2(\mu\text{-dppf})(\mu\text{-S})]\cdot 2\ CHCl_3$ [77] (Fig. 23). A trigonal planar geometry can be disrupted towards a distorted trigonal pyramidal arrangement. Again, the deviation can be accounted for by looking how much the sum of the angles around the metal deviates from 360°. Another way is to measure the shift of the metal atom away from the plane defined by the three phosphorus donor atoms (Δ, in Å). The values for the $[Au_2(\mu\text{-dppf})(\text{dppf})_2Cl_2]\cdot 2\ CH_2Cl_2$ [64] complex (Fig. 17) are 354.8° and 0.31 Å, respectively. In this molecule the gold atom appears then in a distorted trigonal pyramidal geometry.The other compounds with trigonally coordinated Au do not show any gross distortion, and a situation closest to an ideal trigonal coordination is found in $[Au_2(\mu\text{-dppf})(\text{dppf})_2][NO_3]_2\cdot 2\ H_2O$ [65]. In the latter, bond angles around gold sum to 359.7°, $\Delta = 0.07$ Å and P–Au–P angles range from 109.2(1) to 126.8(1)°. It is ascertained, however, that gold(I) chemistry is dominated by the formation of linear molecular coordination compounds, and this is in fact the geometry of the remaining complexes. The compound $[Au_2(\mu\text{-dppf})(\text{pyren-1-yl})_2]$ [74] (Fig. 18) is the first organogold(I)–dppf complex. In this molecule the P–Au–C angle is 172.1(3)°, close to linearity, while in $[Au_2(\text{dppf})(\mu\text{-pdt})]$ [10] (Fig. 22) there is considerable deviation, the P–Au–S angle being as small as 164.7(1)°.

4. There are seven reports of Ru(II) complexes. Four determinations deal with η^5- or η^6-arene Ru(II) compounds: [Ru(dppf)H(Cp*)] [25], $[Ru(\text{dppf})(\eta^6\text{-}Me_6C_6)Cl][PF_6]$ [26a], $[Ru_2(\mu\text{-dppf})(\eta^6\text{-}Me_4\text{–}C_6H_2)_2Cl_4]\cdot CH_2Cl_2$ [26b] and $[Ru(\text{dppf})(\eta^6\text{-}p\text{-cymene})Cl][PF_6]$ [27]. In all these molecules ruthenium shows a three-legged piano-stool coordination. The complex $[Ru(\text{dppf})(\eta^2\text{-}O_2)(Cp^*)][BF_4]$ [28] (Fig. 8) has instead a four-legged piano-stool geometry. In the structures described in [26a,27] the planes defined by the arene ligand and by the P_2Cl base plane are virtually parallel. In fact, the dihedral angle between the two planes is 6.5 and 2.5° in [26a] and 3.1° in [27]. There is instead an angle of 9.8° between the P_2O_2 base plane and the cyclopentadienide plane in [28]. The remaining structures $[Ru(\text{dppf})(\text{bipy})_2][PF_6]_2$ [29], $[Ru(\text{dppf})(CO)(PPh_3)ClH]$ [30] and $[Ru(\text{dppf})(CO)(NCMe)(PPh_3)H][BF_4]\cdot EtOH$ [31] show the octahedral geometry typical of Ru(II) compounds.

References

[1] T. Hayashi, M. Konishi, Y. Kobori, M. Kumada, T. Higuchi, K. Hirotsu, J. Am. Chem. Soc. 106 (1984) 158.
[2] S. Onaka, A. Mizuno, S. Takagi, Chem. Lett. (1989) 2037.
[3] K.-S. Gan, T.S.A. Hor, in: A. Togni, T. Hayashi (Eds.), Ferrocenes — Homogeneous Catalysis, Organic Synthesis and Materials Science, VCH, Weinheim, 1995, p. 3.
[4] S.-W.A. Fong, T.S.A. Hor, J. Clust. Sci. 9 (1998) 351.
[5] F.H. Allen, J.E. Davies, J.J. Galloy, O. Johnson, O. Kennard, C.F. Macrae, E.M. Mitchell, G.F. Mitchell, J.M. Smith, D.G. Watson, J. Chem. Info. Comp. Sci. 31 (1991) 187.
[6] W.-Y. Yeh, Y.-J. Cheng, M.Y. Chiang, Organometallics 16 (1997) 918.

[7] P. Wehman, H.M.A. van Donge, A. Hagos, P.C.J. Kamer, P.V.N.M. van Leeuwen, J. Organomet. Chem. 535 (1997) 183.
[8] P. Zanello, in: A. Togni, T. Hayashi (Eds.), Ferrocenes — Homogeneous Catalysis, Organic Synthesis and Materials Science, VCH, Weinheim, 1995, p. 317.
[9] C.J. McAdam, N.W. Duffy, B.H. Robinson, J. Simpson, J. Organomet. Chem. 527 (1997) 179.
[10] M. Viotte, B. Gautheron, I. Nifant'ev, L.G. Kuz'mina, Inorg. Chim. Acta 253 (1996) 71.
[11] T.-J. Kim, K.-H. Kwon, J.-O. Baeg, S.-C. Shim, J. Organomet. Chem. 389 (1990) 205.
[12] H.S.O. Chan, T.S.A. Hor, L.-T. Phang, K.L. Tan, J. Organomet. Chem. 407 (1991) 353.
[13] L.-T. Phang, S.C.F. Au-Yeung, T.S.A. Hor, S.B. Khoo, Z.-Y. Zhou, T.C.W. Mak, J. Chem. Soc. Dalton Trans. (1993) 165.
[14] M. Sato, M. Sekino, S. Akabori, J. Organomet. Chem. 344 (1988) C31.
[15] M. Sato, H. Shigeta, M. Sekino, S. Akabori, J. Organomet. Chem. 458 (1993) 199.
[16] M.I. Bruce, P.A. Humphrey, O. Shawkataly, M.R. Snow, E.R.T. Tiekink, W.R. Cullen, Organometallics 9 (1990) 2910.
[17] M.C. Gimeno, A. Laguna, C. Sarroca, P.G. Jones, Inorg. Chem. 32 (1993) 5926.
[18] T.S.A. Hor, S.P. Neo, C.S. Tan, T.C.W. Mak, K.W.P. Leung, R.-J. Wang, Inorg. Chem. 31 (1992) 4510.
[19] A.L. Rheingold, B.S. Haggerty, A.J. Edwards, C.E. Housecroft, A.D. Hattersley, N. Hinze, Acta Crystallogr. Sect. C 50 (1994) 1411.
[20] S.C.N. Hsu, W.-Y. Yek, M.Y. Chiang, J. Organomet. Chem. 492 (1995) 121.
[21] M. Sekino, M. Sato, A. Nagasawa, K. Kikuchi, Organometallics 13 (1994) 1451.
[22] S. Onaka, M. Haga, S. Takagi, M. Otsuka, K. Mizuno, Bull. Chem. Soc. Jpn. 67 (1994) 2440.
[23] S. Onaka, H. Furuta, S. Takagi, Angew. Chem. Int. Ed. Engl. 32 (1993) 87.
[24] V. Muneyejabo, J.-P. Damiano, M. Postel, C. Bensimon, J.L. Roustan, J. Organomet. Chem. 491 (1995) 61.
[25] R.T. Hembre, J.S. McQueen, V.W. Day, J. Am. Chem. Soc. 118 (1996) 798.
[26] J.-F. Mai, Y. Yamamoto, J. Organomet. Chem. 560 (1998) 223.
[27] S.B. Jensen, S.J. Rodger, M.D. Spicer, J. Organomet. Chem. 556 (1998) 151.
[28] M. Sato, M. Asai, J. Organomet. Chem. 508 (1996) 121.
[29] V.W.-W. Yam, V.W.-M. Lee, K.-K. Cheung, J. Chem. Soc. Dalton Trans. (1997) 2335.
[30] A. Santos, J. López, J. Montoya, P. Noheda, A. Romero, A.M. Echavarren, Organometallics 13 (1994) 3605.
[31] S.-H. Han, K.-M. Sung, S. Huh, M.-J. Jun, D. Whang, K. Kim, Polyhedron 15 (1996) 3811.
[32] A.E. Gerbase, E.J.S. Vichi, E. Stein, L. Amaral, A. Vasquez, M. Hörner, C. Maichle-Mössmer, Inorg. Chim. Acta 266 (1997) 19.
[33] R.B. Bedford, P.A. Chaloner, P.B. Hitchcock, Acta Crystallogr. Sect. C 49 (1993) 1614.
[34] C.M. de Lima, C.A.L. Filgueiras, M.T.S. Giotto, Y.P. Mascarenhas, Transit. Met. Chem. 20 (1995) 380.
[35] T.F. Baumann, J.W. Sibert, M.M. Olmstead, A.G.M. Barrett, B.M. Hoffmann, J. Am. Chem. Soc. 116 (1994) 2639.
[36] T.F. Baumann, M.S. Nasir, J.W. Sibert, A.J.P. White, M.M. Olmstead, D.J. Williams, A.G.M. Barrett, B.M. Hoffmann, J. Am. Chem. Soc. 118 (1996) 10479.
[37] I.R. Butler, L.J. Hobson, S.J. Coles, M.B. Hursthouse, K.M. Abdul Malik, J. Organomet. Chem. 540 (1997) 27.
[38] C.C.H. Chin, J.S.L. Yeo, Z.H. Loh, J.J. Vittal, W. Henderson, T.S.A. Hor, J. Chem. Soc. Dalton Trans. (1998) 3777.
[39] J.M. Brown, J.J. Pérez-Torrente, N.W. Alcock, H.J. Clase, Organometallics 14 (1995) 207.
[40] M.S. Driver, J.F. Hartwig, J. Am. Chem. Soc. 119 (1997) 8232.
[41] A.S.K. Hashmi, F. Naumann, R. Probst, J.W. Bats, Angew. Chem. Int. Ed. Engl. 36 (1997) 104.
[42] J.F. Hartwig, Angew. Chem. Int. Ed. Engl. 37 (1998) 2090.
[43] T.J. Colacot, R.A. Teichman, R. Cea-Olivares, J.-G. Alvarado-Rodríguez, R.A. Toscano, W.J. Boyko, J. Organomet. Chem. 557 (1998) 169.

[44] D.K. Wicht, M.A. Zhuravel, R.V. Gregush, D.S. Glueck, I.A. Guzei, L.M. Liable-Sands, A.L. Rheingold, Organometallics 17 (1998) 1412.
[45] G.Y. Zheng, D.P. Rillema, J.H. Reibenspies, Inorg. Chem. 38 (1999) 794.
[46] C. Pettinari, F. Marchetti, A. Cingolani, S.I. Troyanov, A. Drozdov, J. Chem. Soc. Dalton Trans. (1998) 3335.
[47] P.J. Stang, B. Olenyuk, J. Fan, A.M. Arif, Organometallics 15 (1996) 904.
[48] G. Vasapollo, L. Toniolo, G. Cavinato, F. Bigoli, M. Lanfranchi, M.A. Pellinghelli, J. Organomet. Chem. 481 (1994) 173.
[49] A.L. Tan, P.M.N. Low, Z.-Y. Zhou, W. Zheng, B.-M. Wu, T.C.W. Mak, T.S.A. Hor, J. Chem. Soc. Dalton Trans. (1996) 2207.
[50] V.C.M. Smith, R.T. Aplin, J.M. Brown, M.B. Hursthouse, A.I. Karalulov, K.M. Abdul Malik, N.A. Cooley, J. Am. Chem. Soc. 116 (1994) 5180.
[51] S.A. Benyunes, L. Brandt, A. Fries, M. Green, M.F. Mahon, T.M.T. Papworth, J. Chem. Soc. Dalton Trans. (1993) 3785.
[52] W.-H. Leung, J.L.C. Chin, W.-T. Wong, J. Chem. Soc. Dalton Trans. (1997) 3277.
[53] G.A. Abakumov, V.K. Cherkasov, A.V. Krashilina, I.L. Eremenko, S.E. Nefedov, Russian Chem. Bull. 47 (1998) 2262.
[54] V.D. Makhaev, F.M. Dolgushin, A.I. Yanovsky, Yu.T. Struchkov, Koord. Khim. 22 (1996) 608.
[55] M.C. Gimeno, P.G. Jones, A. Laguna, C. Sarroca, J. Chem. Soc. Dalton Trans. (1995) 1473.
[56] M.C. Gimeno, A. Laguna, C. Sarroca, P.G. Jones, Inorg. Chem. 32 (1993) 5926.
[57] J. McGinley, V. McKee, C.J. McKenzie, Acta Crystallogr. Sect. C 54 (1998) 345.
[58] B. Longato, R. Coppo, G. Pilloni, C. Corvaja, A. Toffoletti, G. Bandoli, Inorg. Chem., in press.
[59] V. Di Noto, G. Valle, B. Zarli, B. Longato, G. Pilloni, B. Corain, Inorg. Chim. Acta 233 (1995) 165.
[60] B. Longato, L. Riello, G. Bandoli, G. Pilloni, Inorg. Chem. 38 (1999) 2818.
[61] Z.-H. Huang, Z.-X. Huang, H.-H. Zhang, J. Struct. Chem. 16 (1997) 324.
[62] S.P. Neo, Z.-Y. Zhou, T.C.W. Mak, T.S.A. Hor, J. Chem. Soc. Dalton Trans. (1994) 3451.
[63] S.-P. Neo, T.S.A. Hor, Z.-Y. Zhou, T.C.W. Mak, J. Organomet. Chem. 464 (1994) 113.
[64] A. Houlton, D.M.P. Mingos, D.M. Murphy, A.J. Williams, Acta Crystallogr. Sect. C 51 (1995) 30.
[65] L.-T. Phang, T.S.A. Hor, Z.-Y. Zhou, T.C.W. Mak, J. Organomet. Chem. 469 (1994) 253.
[66] J. Granifo, A. Vega, M.T. Garland, Polyhedron 17 (1998) 1729.
[67] S. Onaka, Y. Katukawa, J. Coord. Chem. 39 (1996) 135.
[68] C. Jiang, Y.-S. Wen, L.-K. Liu, T.S.A. Hor, Y.K. Yan, Organometallics 17 (1998) 173.
[69] G. Zhao, Q.-G. Wang, T.C.W. Mak, T.S.A. Hor, J. Chem. Soc. Dalton Trans. (1998) 1241.
[70] J. Díez, M. Pilar Gamasa, J. Gimeno, A. Aguirre, S. García-Granda, J. Holubova, L.R. Falvello, Organometallics 18 (1999) 662.
[71] K. Yang, S.G. Bott, M.G. Richmond, J. Chem. Cryst. 25 (1995) 263.
[72] F. Canales, M.C. Gimeno, P.G. Jones, A. Laguna, C. Sarroca, Inorg. Chem. 36 (1997) 5206.
[73] P.M.N. Low, Z.-Y. Zhang, T.C.W. Mak, T.S.A. Hor, J. Organomet. Chem. 539 (1997) 45.
[74] V.W.-W. Yam, S.W.-K. Choi, K.-K. Cheung, J. Chem. Soc. Dalton Trans. (1996) 3411.
[75] C.J. McAdam, N.W. Duffy, B.H. Robinson, J. Simpson, J. Organomet. Chem. 527 (1997) 179.
[76] M.A. Zhuravel, D.S. Glueck, L.M. Liable-Sands, A.L. Rheingold, Organometallics 17 (1998) 574.
[77] F. Canales, M.C. Gimeno, A. Laguna, P.G. Jones, J. Am. Chem. Soc. 118 (1996) 4839.
[78] M.J. Calhorda, F. Canales, M.C. Gimeno, J. Jiménez, P.G. Jones, A. Laguna, L.F. Veiros, Organometallics 16 (1997) 3837.
[79] F. Canales, M.C. Gimeno, A. Laguna, P.G. Jones, Organometallics 15 (1996) 3412.
[80] J.S.L. Yeo, G. Li, W.-H. Yip, W. Henderson, T.C.W. Mak, T.S.A. Hor, J. Chem. Soc. Dalton Trans. (1999) 435.

[81] M. Zhou, Y. Xu, A.-M. Tan, P.-H. Leung, K.F. Mok, L.-L. Koh, T.S.A. Hor, Inorg. Chem. 34 (1995) 6425.
[82] J.W.-S. Hui, W.-T. Wong, J. Chem. Soc. Dalton Trans. (1997) 2445.
[83] G. Li, S. Li, A.L. Tan, W.-H. Yip, T.C.W. Mak, T.S.A. Hor, J. Chem. Soc. Dalton Trans. (1996) 4315.
[84] J.-F. Ma, Y. Yamamoto, J. Organomet. Chem. 574 (1999) 148.
[85] I.R. Butler, M.G.B. Drew, C.H. Greenwell, E. Lewis, M. Plath, S. Mussig, J. Szewczyk, Inorg. Chem. Comm. 2 (1999) 576.